Biomedicine & Pharmacotherapy 165 (2023) 115066

Contents lists available at ScienceDirect

Biomedicine & Pharmacotherapy

journal homepage: www.elsevier.com/locate/biopha

PLM-101 is a novel and potent FLT3/RET inhibitor with less adverse effects in the treatment of acute myeloid leukemia

Yong June Choi [a], Jaewoo Park [a], Hyoyi Choi [a], Su-Jin Oh [b], Jin-Hee Park [b], Miso Park [a], Ji Won Kim [c], Yoon-Gyoon Kim [d], Yong-Chul Kim [b,e], Myung Jin Kim [b,*], Keon Wook Kang [a,*]

[a] College of Pharmacy and Research Institute of Pharmaceutical Sciences, Seoul National University, Seoul 08826, Republic of Korea
[b] R&D Center, PeLeMed, Co. Ltd., Seoul 06100, Republic of Korea
[c] Jeju Research Institute of Pharmaceutical Sciences, College of Pharmacy, Jeju National University, Jeju 63243, Republic of Korea
[d] College of Pharmacy, Dankook University, Cheonan 31116, Republic of Korea
[e] School of Life Sciences, Gwangju Institute of Science and Technology, Gwangju 61005, Republic of Korea

ARTICLE INFO

Keywords:
AML
RET-mediated autophagic degradation of FLT3
FLT3/RET dual-target inhibitor
Indirubin derivative
PH-dependent solubility

Chemical compounds studied in this article:
PLM-101 (no PubChem CID)
Gilteritinib (PubChem CID: 49803313)
Bafilomycin A1 (PubChem CID: 117059119)
Chloroquine phosphate (PubChem CID: 64927)
Metoclopramide hydrochloride (PubChem CID: 23659)
Famotidine (PubChem CID: 5702160)

ABSTRACT

Acute myeloid leukemia (AML) is a prevalent form of leukemia in adults. As its survival rate is low, there is an urgent need for new therapeutic options. In AML, *FMS-like tyrosine kinase 3* (*FLT3*) mutations are common and have negative outcomes. However, current FLT3-targeting agents, Midostaurin and Gilteritinib, face two significant issues, specifically the emergence of acquired resistance and drug-related adverse events leading to treatment failure. *Rearranged during transfection* (*RET*), meanwhile, is a proto-oncogene linked to various types of cancer, but its role in AML has been limited. A previous study showed that activation of RET kinase enhances FLT3 protein stability, leading to the promotion of AML cell proliferation. However, no drugs are currently available that target both FLT3 and RET. This study introduces PLM-101, a new therapeutic option derived from the traditional Chinese medicine *indigo naturalis* with potent *in vitro* and *in vivo* anti-leukemic activities. PLM-101 potently inhibits FLT3 kinase and induces its autophagic degradation *via* RET inhibition, providing a superior mechanism to that of FLT3 single-targeting agents. Single- and repeated-dose toxicity tests conducted in the present study showed no significant drug-related adverse effects. This study is the first to present a new FLT3/RET dual-targeting inhibitor, PLM-101, that shows potent anti-leukemic activity and fewer adverse effects. PLM-101, therefore, should be considered for use as a potential therapeutic agent for AML.

1. Introduction

Acute myeloid leukemia (AML) is a hematopoietic malignancy characterized by abnormal differentiation and proliferation of myeloid lineage cells. AML is the most prevalent type of leukemia in adults, accounting for nearly 30% of all adult leukemia cases [1–3]. Due to the low 5-year survival rate of AML patients, estimated at only 30%, there is an urgent need to develop effective treatment options for this hematopoietic disease [4,5]. In recent years, significant progress has been made in understanding the genetic alterations that underlie AML [6–8]. These advances have opened up new opportunities for the development of therapeutic options for AML [9,10].

FMS-like tyrosine kinase 3 (FLT3) is one of the most frequently mutated genes in AML, and its various mutations are associated with poor overall survival and disease-free survival [11–13]. *FLT3* mutations occur in approximately 30% of all AML cases, which include internal tandem duplication mutations (*FLT3*-ITD mutation; approximately 25% of all AML cases) in the juxtamembrane or tyrosine kinase 1 domain, and point mutations in the tyrosine kinase 2 domain (*FLT3-TKD* mutation; approximately 8% of all AML cases) [6,14]. Due to the high frequency of

Abbreviations: AML, acute myeloid leukemia; FLT3, FMS-like tyrosine kinase 3; FLT3-ITD, FLT3-internal tandem duplication; FLT3-TKD, FLT3-tyrosine kinase domain; FDA, Food and Drug Administration; RET, rearranged during transfection; NSCLC, non-small cell lung cancer; PTC, papillary thyroid cancer; mTORC1, mammalian target of rapamycin complex 1; ULK1, Unc-51-like autophagy activating kinase 1; TCM, traditional Chinese medicine; PI3K, phosphoinositide 3-kinase; ERK, extracellular signal-regulated kinase; TUNEL, terminal deoxynucleotidyl transferase dUTP nick end labeling; NSGA, NOD/ShiLtJ-*Prkdc*^{em1AMC}*Il2rg*^{em1AMC}; SGF, simulated gastric fluid; FeSSIF, fed-state simulated intestinal fluid; FaSSIF, fasted-state simulated intestinal fluid.

* Corresponding authors.
E-mail addresses: mjkim@pelemed.com (M.J. Kim), kwkang@snu.ac.kr (K.W. Kang).

https://doi.org/10.1016/j.biopha.2023.115066
Received 24 April 2023; Received in revised form 12 June 2023; Accepted 23 June 2023
Available online 29 June 2023

FLT3 mutations in AML, targeted therapies mainly for FLT3 are under development [15–17]. Although two FLT3-targeting agents, Midostaurin and Gilteritinib, have been approved by the U.S. Food and Drug Administration (FDA) for patients with relapsed/refractory *FLT3*-mutated AML [18,19], they have faced two critical setbacks. The first is the emergence of secondary mutations in the *FLT3* gene, such as D835Y or F691L, leading to acquired resistance against the targeted therapy [20,21]. The second is the occurrence of drug-related adverse events, including hepatotoxicity, hematologic toxicity (febrile neutropenia, anemia, and thrombocytopenia), and cardiac toxicity (prolonged QT intervals), which can cause treatment failure [22–24]. These two critical issues require urgent attention.

Rearranged during transfection (RET), meanwhile, is one of the proto-oncogenes encoding a receptor tyrosine kinase that is associated with the proliferation and survival of various types of cancer [25–28]. Although the function of RET fusion and rearrangement is well established in non-small cell lung cancer (NSCLC) and papillary thyroid cancer (PTC), its role in AML has been limited [29]. Recently, several studies have shown that RET expression correlates with poor prognosis in AML patients [30,31]. Furthermore, RET activation promotes proliferation of AML cells through direct or indirect mechanisms, such as stabilization of FLT3 protein [31]. Hence, investigating the role of RET and its potential application as a pharmacological intervention in AML is becoming increasingly important.

Autophagy recently has been found to play an important role in the post-translational degradation of FLT3 [32–35]. Larrue et al. demonstrated that Bortezomib, a proteasome pathway inhibitor, can activate autophagy and subsequently lead to degradation of FLT3 in AML cells [34]. Moreover, the highly activated RET in AML cells can activate mammalian target of rapamycin complex 1 (mTORC1), resulting in the inactivation of Unc-51-like autophagy activating kinase 1 (ULK1), leading to the inhibition of autophagic degradation of FLT3 [31]. Indeed, combination of FLT3 inhibitor Crenolanib with an RET inhibitor such as Vandetanib or Danusertib, significantly reduces the cell viability of *FLT3*-ITD-mutated AML cell lines *via* induction of autophagic degradation of FLT3 [31]. Thus, RET-targeting may be a valuable therapeutic strategy for *FLT3*-mutant AML with RET activation. However, there are currently no FLT3/RET dual-targeting drugs, and only a limited number of RET-targeting drugs have been approved for clinical use [36].

In this study, we propose PLM-101, a synthetic derivative of indirubin from the traditional Chinese medicine (TCM) *indigo naturalis*, as a promising anti-leukemic therapeutic option. This compound demonstrated strong inhibitory activity against acquired-resistant mutations such as D835Y and F691L. Its pharmacological mechanism is the inhibition of FLT3 and its downstream signaling pathways, including the phosphoinositide 3-kinase (PI3K)/AKT and Ras/extracellular signal-regulated kinase (ERK) pathways. Additionally, PLM-101 induces autophagic degradation of FLT3 by targeting RET, thus providing an additional mechanism to the stronger anti-leukemic activity of FLT3/RET dual-targeting inhibitors relative to that of FLT3 single-targeting inhibitors. In toxicity tests, no significant drug-related adverse effects against the liver or blood were observed. This study presents a novel FLT3/RET dual-targeting inhibitor, PLM-101, that exhibits potent anti-leukemic activity with less adverse effects. PLM-101, therefore, should be considered as a potential therapeutic option for acute myeloid leukemia harboring both *RET* and *FLT3* mutations.

2. Materials and methods

2.1. Cell lines

Human AML cell lines MV4–11, MOLM-13, and MOLM-14 were donated by professor Yong-Chul Kim (Gwangju Institute of Science and Technology, Gwangju, South Korea). The U-937 and HL-60 AML cell lines were obtained from the Korean Cell Line Bank (Seoul, South Korea). MV4–11, MOLM-13, MOLM-14, and U-937 cells were maintained in RPMI 1640 medium supplemented with 10% fetal bovine serum (FBS, #16000–044, Thermo Fisher Scientific, Waltham, MA, USA) and 1% penicillin/streptomycin solution (#SV30010, Hyclone, Logan, UT, USA), while the HL-60 AML cell line was maintained in Iscove's Modified Dulbecco's Medium (IMDM) supplemented with 10% FBS and 1% penicillin/streptomycin solution. All cell lines were cultured in a humidified incubator at 37 ℃ with 5% CO_2.

2.2. Chemicals and antibodies

The PLM-101 compound was donated from PeleMed (Seoul, South Korea). Gilteritinib (#HY-12432) was purchased from MedChemExpress (Monmouth Junction, NJ, USA). Bafilomycin A1 (#B1793), Chloroquine phosphate (#PHR1258), Metoclopramide hydrochloride (#M0763), Famotidine (#PHR1055) and β-actin antibody (#A2228) were supplied from Sigma-Aldrich (St. Louis, MO, USA). All compounds used for *in vitro* study were dissolved in dimethyl sulfoxide (DMSO) and stored at − 20 ℃ until use. Primary antibodies against FLT3 (#3462 S), phopho-FLT3 tyr589/591 (#3464 S), RET (#3220 S), PARP/cleaved-PARP (#9532 S), Caspase-3 (#9662 S), cleaved-Caspase-3 (#9664 S), Cyclin D1 (#2978 S), SQSTM1/p62 (#5114 S), LC3B (#2775 S), AKT (#9272 S), phospho-AKT ser473 (#9271 S), p70S6K (#9202 S), phospho-p70S6K thr389 (#9234 S), mitogen-activated protein kinase kinase (MEK)1/2 (#8727 S), phospho-MEK1/2 ser217/221 (#9154 S), extracellular signal-regulated kinase (ERK)1/2 (#9102 S), phospho-ERK1/2 thr202/tyr204 (#9101 S), phospho-mTOR ser2448 (#2971), and phospho-ULK1 ser555 (#5869) were purchased from Cell Signaling Technology (Danvers, MA, USA). Glyceraldehyde 3-phosphate dehydrogenase (GAPDH) antibody (#CB1001) was obtained from Merck Millipore (Burlington, MA, USA). Antibodies against Cyclin B1 (#sc-245), Cyclin E (#sc-377100), p21 (#sc-6246), and p53 (#sc-6243) were purchased from Santa Cruz Biotechnology (Dallas, TX, USA). Horseradish peroxidase (HRP)-linked secondary antibodies against anti-rabbit IgG (#7074 S) and anti-mouse IgG (#7076 S) were purchased from Cell Signaling Technology (Danvers, MA, USA). Antibodies used for flow cytometry included APC/Cy7 anti-human CD45 (#304014, BioLegend, San Diego, CA, USA) and APC anti-human RET (#IC718A, R&D Systems, Minneapolis, MN, USA). IVISbrite D-luciferin potassium salt (#122799, PerKinElmer, Waltham, MA, USA) was used to determine *in vivo* luminescence.

2.3. In vitro kinase activity assay

The inhibitory activities of various kinases were measured using the HTRF KinEASE-TK kit (Cisbio, Codolet, France) as described in previous studies [37,38]. Briefly, 1 ng of kinase enzyme was reacted with 100 μM ATP, 0.1 μM kinase substrate, and serially diluted inhibitor in a kinase reaction buffer (50 mM HEPES, pH 7.0, 0.1 mM orthovanadate, 5 mM $MgCl_2$ 1 mM DTT, 0.01% BSA, 0.02% NaN_3). The time-resolved fluorescence energy transfer (TR-FRET) signal was measured by Victor multi-label reader (PerkinElmer). The IC_{50} values were calculated using GraphPad Prism 7.0 (GraphPad Software Inc, San Diego, CA, USA).

2.4. Ba/F3 proliferation assay

Each of the FLT3-mutant overexpressing Ba/F3 cells were seeded in 96-well plates (3×10^3 cells/well) and treated with serially diluted PLM-101 or Gilteritinib. After 72 h incubation, cell viability was measured using CellTiter-Glo (#G7573, Promega, Madison, WI, USA). The GI_{50} values were calculated using GraphPad Prism 7.0.

2.5. WST-8 assay: cell viability assay

AML cells were seeded in 96-well plates (5×10^3 cells/well) and were treated with PLM-101 or Gilteritinib. After 72 h incubation, 10 μL WST-8 solution (#CM-VA1000, Precaregene, Anyang, South Korea) were added

and incubated for additional 4 h in the dark. The absorbance at 450 nm was measured using a multi-mode microplate reader (SpectraMax iD3, Molecular Devices, San Jose, CA, USA) to calculate the number of viable cells. The IC_{50} value were analyzed using GraphPad Prism 7.0.

2.6. Apoptosis and cell cycle analysis by flow cytometry

AML cells were seeded in 6-well plates (5 $\times 10^5$ cells) and treated with PLM-101 or Gilteritinib. After 24 h drug treatment, AML cells were washed with cold PBS and re-suspended in 70% ethanol in PBS, and incubated at − 20 ℃ for 24 h for fixation. After fixation, cells were stained in the staining buffer containing 0.2% propidium iodide solution (#P4864, Sigma-Aldrich), 0.1% RNase A solution (#12091–039, Invitrogen, Waltham, CA, USA), and 0.1% triton-X100 (#T8532, Sigma-Aldrich) for 30 min at room temperature in the dark. The DNA contents of the AML cells were analyzed by flow cytometry (Novocyte, Agilent, Santa Clara, CA, USA) according to the manufacturer's protocol.

2.7. Western blot analysis

After treatments, cells were lysed in a lysis buffer containing 10 mM Tris-Cl, 1% Triton X-100, 100 mM sodium chloride, 10% glycerol, 1 mM EDTA, 30 mM sodium pyrophosphate, 5 mM glycerol-2-phophate, 1 mM sodium fluoride, 1 mM sodium orthovanadate, 1% phosphatase inhibitor cocktail 2 (#P5726, Sigma-Aldrich), 1% phosphatase inhibitor cocktail 3 (#P0044, Sigma-Aldrich), and 0.02 tablet/mL protease inhibitor cocktail (#11697498001, Roche, Basel, Switzerland). The protein concentrations of the supernatants were quantified by bradford assay. Protein samples were separated on SDS-polyacrylamide gels and transferred to 0.45 μm nitrocellulose membranes (#10600002, Cytiva, Marlborough, MA, USA). The membranes were blocked with 5% skim milk in PBST (phosphate-buffered saline with 0.1% tween 20) and incubated with primary antibodies overnight at 4 ℃. After overnight incubation, the membranes were washed and incubated with secondary antibodies at room temperature. Membranes were developed using a chemiluminescent HRP substrate (#WBKLS0500, Merck Millipore) and were detected by LAS-3000 mini (Fujifilm, Tokyo, Japan). All immunoblotting results were repeated independently for a minimum of three times, and the densitometry data for each result can be found in Fig. S5.

2.8. mRNA isolation and real-time polymerase chain reaction (PCR)

Total RNA was isolated using Trizol reagent (#15596018, Invitrogen), chloroform, and absolute ethanol according to the manufacturer's protocol. cDNA was synthesized from 1 μg total RNA using the Maxime RT PreMix kit (#25081, IntronBio, Seongnam, South Korea) and quantitative PCR was performed with SYBR green supermix (#1708884, Bio-Rad laboratories, Hercules, CA, USA) using the CFX Connect Real-Time PCR System (Bio-Rad laboratories). The specific primer sequences are as follows: human *FLT3* forward primer 5′-TGGACCTTCTCTCGAAAATCATTT-3′, human *FLT3* reverse primer 5′-GCATCATCATTTTCTGCATGGA-3′, human *RET* forward primer 5′-GAGAAGCTCAGTGTCCGC-3′, human *RET* reverse primer 5′-GGAGGTGTTGAAGAAGGAGAAG-3′, human *GAPDH* forward primer 5′-CTCTGCTCCTCCTGTTCGAC-3′, human *GAPDH* reverse primer 5′-ACCAAATCCGTTGACTCCGA-3′.

2.9. Small interfering RNA (siRNA) transfection

Specific knockdown of *FLT3* and *RET* was achieved using siRNAs with Lipofectamine 2000 transfection reagents (#11668027, Thermo Fisher Scientific, Waltham, MA, USA) according to the manufacturer's instructions. Predesigned *siRET* pools (No. 5979–1,2,3) and negative control siRNA (#SN-1001) were supplied from Bioneer (Daejeon, South Korea).

2.10. Autophagosome detection

Autophagosome were detected using CYTO-ID Autophagy Detection Kit (#ENZ-KIT175–0200, Enzo Life Science, Farmingdale, NY, USA) according to the manufacturer's protocol. Briefly, after treating cells with PLM-101 or *RET* specific knockdown, the amount of autophagosomes in cells was detected by flow cytometry (Novocyte, Agilent). 0.5 μM rapamycin was used as a positive control according to the protocol.

2.11. Pharmacokinetics study

To determine the pharmacokinetic profile of PLM-101, 7–9 week-old male ICR mice were intravenously (IV) or orally (PO) administered with PLM-101. Blood was collected (approximately 0.03 mL per time point) from the saphenous vein into pre-chilled commercial EDTA-K2 tubes. Blood samples were processed for plasma sampling by centrifugation at 3,200 g at 4 ℃ for 10 min. The plasma was collected and transferred into a 96-well plate for LC-MS/MS analysis. To measure plasma concentrations of repeated doses of PLM-101, C57BL/6 J mice were orally administered with PLM-101 once daily for two weeks. On days 7 and 14, mice were sacrificed and blood samples were collected by cardiac puncture. All procedures were approved by the Institutional Animal Care and Use Committee of Seoul National University (Approval #SNU-220918–2) and mice were obtained from Raonbio (Seoul, South Korea).

2.12. flank xenograft mouse model

MV4–11 or MOLM-14 cells (1 $\times 10^7$) were suspended in 100 μL of PBS and subcutaneously injected into the flanks of 6-week-old male BALB/c-nu mice. When the tumor became palpable (100 ~ 150 mm^3), the mice were randomized into the experiment groups. PLM-101 and vehicle were administered by oral gavage (PO) once a day for the indicated days. Tumor volume and body weight were measured every three days. Tumor volume was calculated using a caliper as the following formula: length x ($width^2$) x 0.5. For immunoblotting and terminal deoxynucleotidyl transferase dUTP nick end labeling (TUNEL) assay, mice were administered with PLM-101 for 5 days after the tumor volume reached 500 mm^3, and then sacrificed for tumor tissue sampling. All procedures were approved by the Institutional Animal Care and Use Committee of Seoul National University (Approval #SNU-220621–6). Mice were obtained from JA BIO (Suwon, South Korea) and housed in a specific-pathogen-free facility at the Seoul National University Institute of Laboratory Animal Resources.

2.13. Orthotopic xenograft mouse model

To generate MV4–11-luc or MOLM-14-luc cells, lentiviral particles containing the CMV-Luciferase (firefly) gene (#LVP009, AMSBIO, Cambridge, MA, USA) were transduced into MV4–11 or MOLM-14 cells, respectively. MV4–11-luc or MOLM-14-luc cells (1 $\times 10^6$) were suspended in 100 μL of PBS and injected *via* the tail-vein into 6-week-old male NOD/ShiLtJ-*Prkdc*^{em1AMC}*Il2rg*^{em1AMC} (NSGA) mice. Four days after cell injection, the mice were randomly assigned to experiment groups and drug administration was initiated. PLM-101 or vehicle was administered by oral gavage (PO) once a day for the indicated days. Bioluminescence intensity was detected every week using IVIS Spectrum In Vivo Imaging System (PerkinElmer). Before bioluminescence detection, 150 mg/kg D-Luciferin Potassium Salt (#122799, PerkinElmer) were intraperitoneally injected into the mice 10 min prior. To collect metastasized AML cells in each organ, the organ tissues were dissociated using the gentleMACS dissociator (Miltenyi Biotec, Bergisch Gladbach, Germany). The total immune cell population was obtained from ground tissue using a 33% percoll solution according to the reference protocol [39]. The collected immune cells were stained with APC/Cy7 anti-human CD45, APC anti-human RET, and FITC-labeled autophagosome detection kit. The stained cells were analyzed by flow cytometry

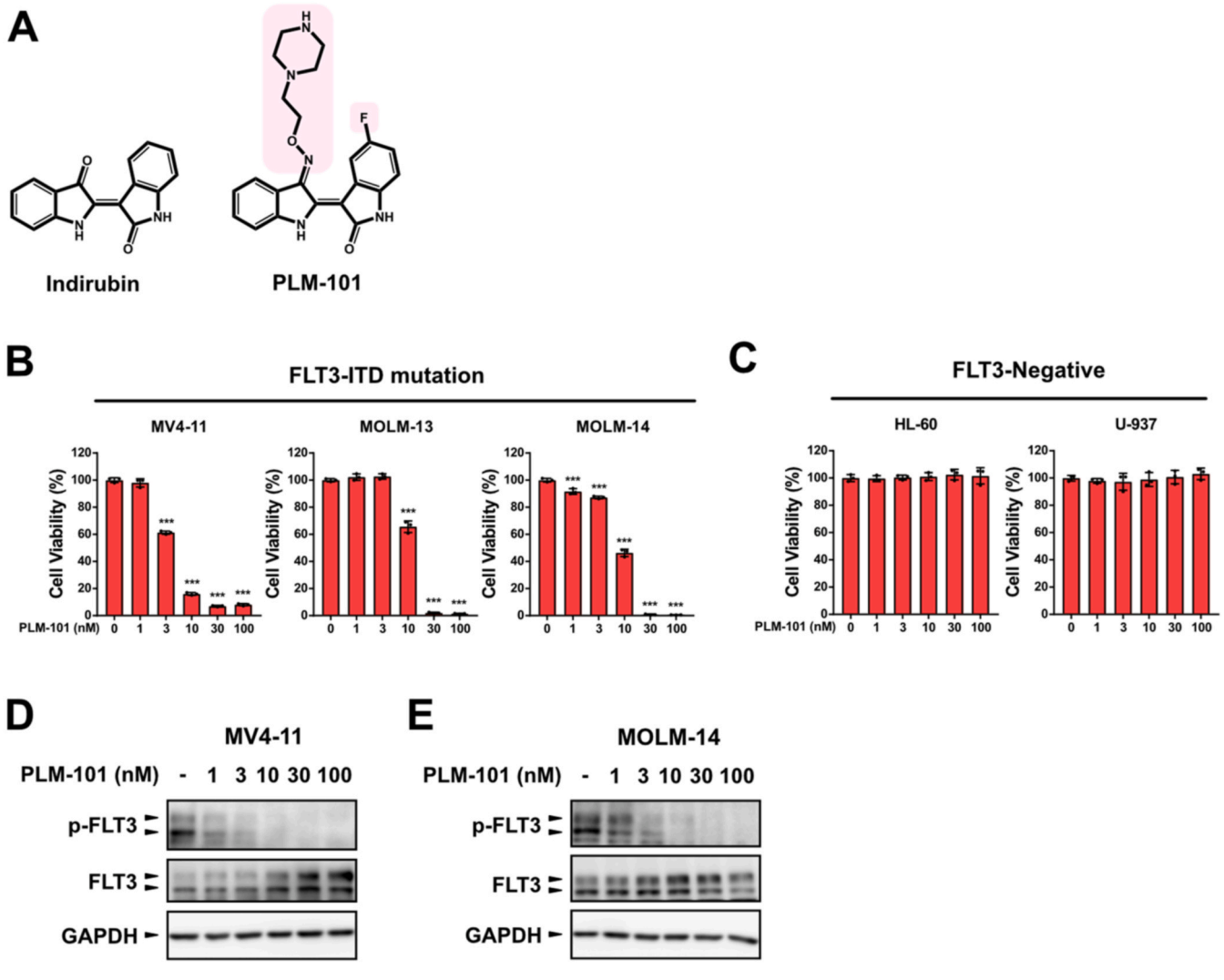

Table 1

FLT3 inhibitor		PLM-101	Gilteritinib
FLT3 Kinase Activity (IC50, nM)	FLT3-ITD	0.565	0.576
BaF3-FLT3 (GI50, nM)	FLT3-ITD	0.7	1.6
	FLT3-ITD-D835Y	0.7	1.5
	FLT3-ITD-F691L	10.5	22.5
RET Kinase Activity (IC50, nM)	RET	0.849	3.57
	RET-M918T	0.838	4.85

Table2

Cell line	IC50 (nM) (95% CI)	
	PLM-101	Gilteritinib
MV4-11	3.26 (2.99-3.76)	8.28 (7.11-9.49)
MOLM-13	10.47 (ND)	25.82 (ND)
MOLM-14	9.64 (9.23-10.08)	17.54 (15.57-19.29)
HL-60	-	-
U-937	-	-

Fig. 1. The discovery of a compound that has anti-leukemic effects and targets FLT3 and RET kinase. (A) The structure of the PLM-101, derivative of indirubin. The boxed part is the converted part of the substituent. (B) Anti-leukemic activity of PLM-101 against FLT3-ITD-mutant AML cell lines using the WST-8 assay. (C) Anti-leukemic activity of PLM-101 against FLT3-negative AML cell lines using the WST-8 assay. In Fig. B and C, PLM-101 was treated for 72 h at the indicated concentration. (D, E) Inhibition of FLT3 activity (phospho-Y589/Y519 of FLT3) by PLM-101. In Fig. D and E, PLM-101 was treated for 3 h at the indicated concentration. All data represent the mean ± SD. Statistical significance of the differences in Fig. B and C was determined by one-way ANOVA followed by the Tukey's test. * ** , $P < 0.001$ significant as compared with control group.

(Novocyte, Agilent). All procedures were approved by the Institutional Animal Care and Use Committee of Seoul National University (Approval #SNU-211022–5).

2.14. Immunohistochemistry (IHC): TUNEL assay

Tumor tissues from xenografts were fixed in 4% paraformaldehyde and embedded in paraffin. Paraffin-embedded tumor tissue slides were immunostained using the TUNEL assay kit (#S7100, Merck Millipore). The images were captured using Fluorescence Microscope (Olympus IX70, Olympus, Tokyo, Japan).

2.15. Single dose and repeated dose toxicity

7–9 week-old male ICR mice were given daily oral doses of PLM-101, and general symptoms such as death were monitored for two weeks. After the administration period ended, biochemical indices in blood samples and histopathological tests were conducted.

2.16. Inhibition of PLM-101 absorption by co-administration with Metoclopramide and Famotidine

C57BL/6 J mice were fasted for 12 h. Metoclopramide and Famotidine were used to induce increased gastric emptying rate and gastric pH, respectively. 10 mg/kg Metoclopramide and 10 mg/kg Famotidine were injected by intraperitoneally 30 min before the oral administration of PLM-101. 2 h after PLM-101 administration, mice were sacrificed and blood samples were collected by cardiac puncture to measure the drug concentration in the plasma. All procedures were approved by the Institutional Animal Care and Use Committee of Seoul National University (Approval #SNU-220621–5) and mice were obtained from Raonbio (Seoul, South Korea).

2.17. in vitro solubility assay

21.8 mg of the PLM101-HCl salt was weighed into each 20 mL glass vial. 10 mL of each solubility medium was added. The amount of HCl salt used is equivalent to 20 mg in anhydrous free form. The obtained solution was stirred at 37 ℃ at 400 rpm for 2 h and 24 h, and centrifuged at 37 ℃ at 14,000 rpm for 5 min. The supernatant was analyzed for solubility and the pH by high performance liquid chromatography (HPLC) and pH meter, respectively.

2.18. Cytochrome p450 (CYP) inhibition

The inhibition effects of PLM-101 on each CYP enzyme activity was measured using human liver microsomes at a concentration of 0.25 mg/mL. A substrate drug cocktail consisting of five drugs (50 μM phenacetin, 10 μM diclofenac, 100 μM S-mephenytoin, 5 μM dextromethorphan, and 2.5 μM midazolam), and 0.1 M phosphate buffer at pH 7.4 was added to the microsomes, and the mixture was incubated for 5 min. Then, a NADPH generation system solution was added, and the reaction was allowed to proceed at 37 ℃ for 15 min. The supernatant of the reacted mixture was analyzed using LC-MS/MS.

2.19. Plasma protein binding assay

5 μM PLM-101 was reacted with plasma in a shaking incubator (37 ℃, 4 h). After the reaction, plasma samples were collected, and cold acetonitrile-containing internal standard was added to terminate the reaction. 100 μL supernatant was analyzed by LC-MS/MS. To calculate the ratio of drug bound to plasma protein, we used the following formula: Free form (%) = (buffer chamber / plasma chamber) x 100; Bound form (%) = 100 - Free form (%).

Table 1
In vitro kinase activity assay and BaF3 proliferation assay for different FLT3 and RET kinase forms.

FLT3 inhibitor		PLM-101	Gilteritinib
FLT3 Kinase Activity (IC_{50}, nM)	FLT3-ITD	0.565	0.576
BaF3-FLT3 (GI_{50}, nM)	FLT3-ITD	0.7	1.6
	FLT3-ITD-D835Y	0.7	1.5
	FLT3-ITD-F691L	10.5	22.5
RET Kinase Activity (IC_{50}, nM)	RET	0.849	3.57
	RET-M918T	0.838	4.85

Table 2
The IC_{50} values of figure B and C.

Cell line	IC_{50} (nM) (95% CI)	
	PLM-101	**Gilteritinib**
MV4–11	3.26 (2.99–3.76)	8.28 (7.11–9.49)
MOLM-13	10.47 (ND)	25.82 (ND)
MOLM-14	9.64 (9.23–10.08)	17.54 (15.57–19.29)
HL-60	-	-
U-937	-	-

2.20. Statistical analysis

The statistical analyses were performed using GraphPad Prism 7.0. Unpaired two-tailed Student t-test or one-way ANOVA followed by the Tukey's test were used to analyze the significance between groups. *P* values less than 0.05 were considered as significant difference. *P* value style was used as NEJM; *p ≤ 0.05, * *p < 0.01, * **p < 0.001.

3. Results

3.1. Identification of anti-leukemic compound targeting FLT3 and RET

PLM-101 (Fig. 1A) has been identified as an FLT3 inhibitor during screening of diverse indirubin derivatives [40]. In order to verify whether PLM-101, one of the indirubin derivatives, can target both FLT3 and RET kinase activities, *in vitro* kinase activity and Ba/F3 proliferation assays were performed in the current study. Currently, only Gilteritinib has been approved by the U.S. FDA as a selective FLT3 inhibitor for relapsed/refractory *FLT3*-ITD-mutated AML patients [24]. Therefore, Gilteritinib was used for comparison. PLM-101 showed strong inhibitory activities against mutant FLT3 kinase and RET kinase with IC_{50} of 0.565 nM and 0.849 nM, respectively. Additionally, it inhibited the proliferation of Ba/F3 cells expressing FLT3-ITD-mutant kinases at the nanomolar (nM) concentration levels (Table 1). Specifically, it was found that the inhibition of RET kinase activity by PLM-101 was significantly superior to that of Gilteritinib, based on IC_{50} of 0.849 nM and 3.57 nM, respectively (Table 1). Moreover, PLM-101 exhibited robust inhibitory activity against the D835Y and F691L secondary mutants, suggesting its potential effectiveness against mutations that cause acquired resistance to FLT3 inhibitors (Table 1). The *FLT3*-ITD mutation is responsible for approximately 25% of all AML cases and is associated with poor overall survival [6]. Thus, we confirmed the anti-proliferation activities of PLM-101 against *FLT3*-ITD-positive AML cell lines (MV4–11, MOLM-14, and MOLM-13). PLM-101 exhibited more potent anti-leukemic activity that did Gilteritinib (Figs. 1B, S1A, Table 2). However, neither PLM-101 nor Gilteritinib showed anti-proliferation effects in *FLT3*-negative AML cell lines (U-937 and HL-60, Figs. 1C, S1B, Table 2). The decreased phosphorylation Y589/Y519 in FLT3 kinase confirmed that FLT3 kinase activity can be effectively suppressed in *FLT3*-ITD-positive AML cell lines by treatment with PLM-101 (Fig. 1D, E). These results suggested

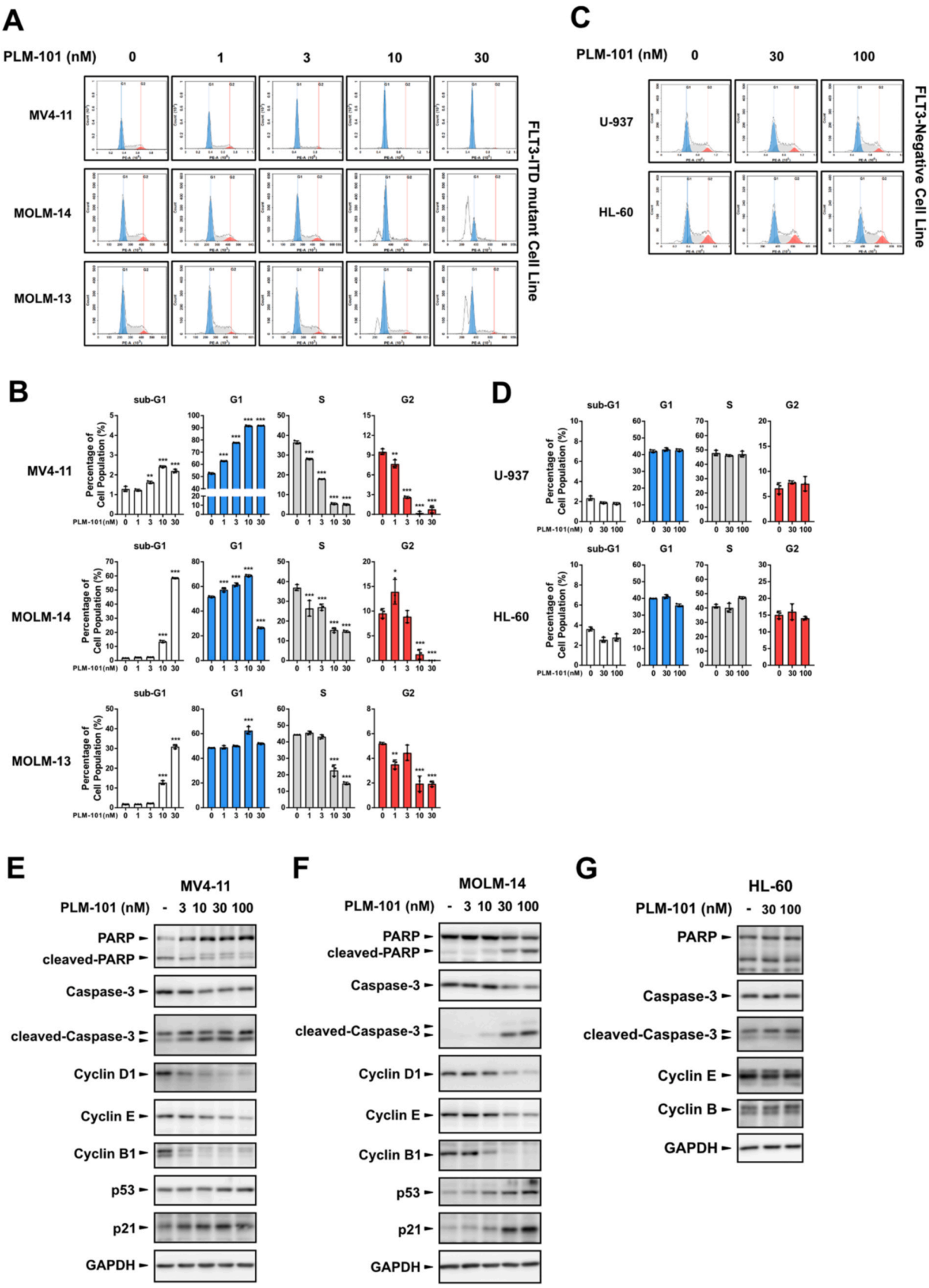

Fig. 2. The induction of apoptosis and cell cycle arrest by PLM-101. (A, C) The measurement of intracellular DNA levels through propidium iodide staining following PLM-101 treatment using flow cytometry. **(B, D)** The Calculation of the percentage in various stages of the cell cycle. (E, F, G) The alterations in markers of apoptosis (cleaved-PARP, cleaved-caspase-3) and cell cycle (cyclin D1, E, B1, p53, p21) cause by PLM-101 treatment. In all figures, PLM-101 was treated for 24 h at the indicated concentration. All data represent the mean ± SD. Statistical significance of the differences in Fig. B and D was determined by one-way ANOVA followed by the Tukey's test. * , $P < 0.05$, * *, $P < 0.01$, * ** , $P < 0.001$ significant as compared with control group.

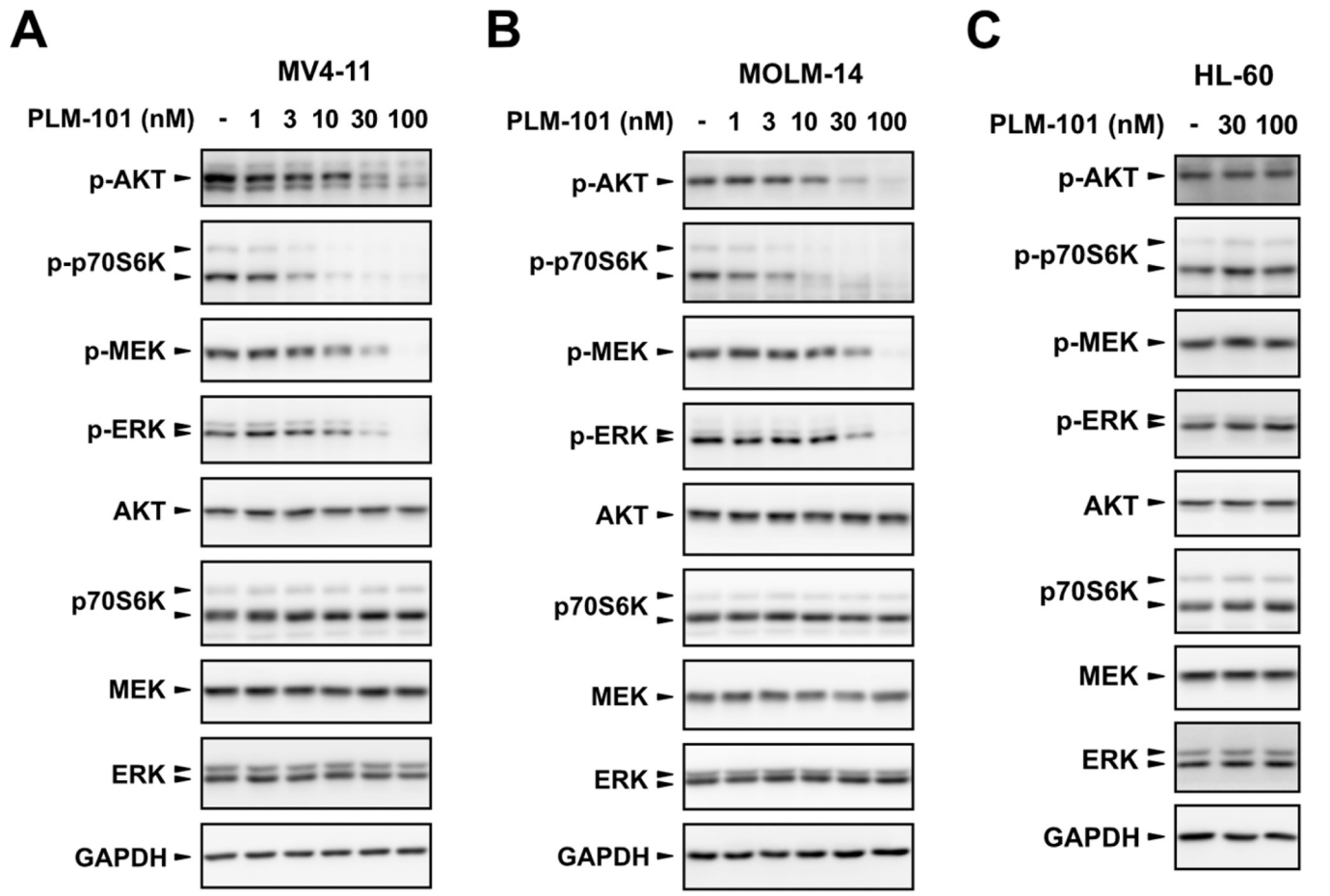

Fig. 3. The anti-leukemic effects of PLM-101 achieved through the suppression of PI3K and Ras signaling pathway. (A, B) Inhibition of PI3K pathway (phospho-S473 AKT and phospho-T389 p70S6K) and Ras pathway (phospho-S217/S221 MEK and phospho-T202/Y204 ERK) by PLM-101 in FLT3-ITD-mutant AML cell lines. (C) Inhibition of PI3K pathway and Ras pathway by PLM-101 in FLT3-negative AML cell line. In all figures, PLM-101 was treated for 3 h at the indicated concentration.

that PLM-101, a novel dual-targeting inhibitor of FLT3 and RET kinase, has potent anti-leukemic activity.

3.2. Apoptosis induction and cell cycle arrest by PLM-101

To evaluate the effects of PLM-101 on apoptosis and cell cycle arrest in *FLT3*-ITD-positive AML cell lines, intracellular DNA contents were analyzed by flow cytometry 24 h after drug treatment. Similar to the cell viability results, strong apoptosis and cell cycle arrest effects of PLM-101 were confirmed in *FLT3*-ITD-positive AML cell lines (Fig. 2A-2D). After 24 h exposure to PLM-101, the cleaved forms of PARP and caspase-3, which are representative markers of apoptosis, were observed (Fig. 2E, F). Furthermore, decreased levels of Cyclin D1, Cyclin E, and Cyclin B1 along with increased levels of p53 and p21, indicative of cell cycle arrest induction, were observed (Fig. 2E, F). However, no such changes occurred in the *FLT3*-negative AML cell line, HL-60 (Fig. 2 G). The apoptosis and cell cycle arrest effects of the positive control agent, Gilteritinib, in *FLT3*-ITD-positive AML cell lines were similarly confirmed (Fig. S1C-F).

3.3. Anti-leukemic activity of PLM-101 via inhibition of PI3K and Ras/ERK signaling pathways

A previous study established the pivotal role of FLT3 in the growth and proliferation of AML cells by activation of PI3K/AKT and Ras/ERK signaling pathways [41]. FLT3 inhibitors such as Gilteritinib have been found to inhibit the activities of downstream components of the PI3K and Ras signaling pathways [42,43]. To verify the mechanism underlying the anti-leukemic activity of PLM-101, we examined the activities of the PI3K and Ras signaling pathways. Similar to other FLT3 inhibitors, PLM-101 suppressed the phosphorylation of AKT (phospho-S473) and p70S6K (phospho-T389) in the PI3K signaling pathway, as well as the phosphorylation of MEK (phospho-S217/S221) and ERK (phospho-T202/Y204) in the Ras signaling pathway (Fig. 3A, B). However, no inhibitory activity was observed in the *FLT3*-negative AML cell line, HL-60 (Fig. 3C). Thus, we concluded that PLM-101 exerts anti-leukemic activity by inhibiting the signal transduction of the FLT3-ITD mutant protein, similarly to other FLT3 inhibitors.

3.4. PLM-101 inhibition of RET kinase affects the stability of FLT3-ITD protein via the autophagy pathway

Recent studies have highlighted the crucial role of RET in AML [30,31]. RET-mediated autophagy suppression has been suggested as a potential target for AML treatment [31]. In the present study then, prior to evaluating the effect of RET-targeting in AML cells, the expression level of RET protein was assessed in AML cell lines. Among the tested AML cell lines, RET was expressed only in MOLM-14 cells (Figs. 4A, S2A, B). Treatment of PLM-101 to RET-positive MOLM-14 led to degradation of RET and FLT3 proteins with an increase in autophagy markers, specifically a decrease in p62 and an increase in LC3B-2/LC3B-1 ratio and LC3B-2 proteins. However, the activation of the autophagy markers was not observed in RET-negative MV4–11 and HL-60 cells treated with PLM-101 (Figs. 4B, C, D, S2C, D). The PLM-101-induced degradation of RET and FLT3 was reversed by co-treatment with autophagy inhibitor, Bafilomycin or Chloroquine (Fig. 4E, F). In RET-positive MOLM-14,

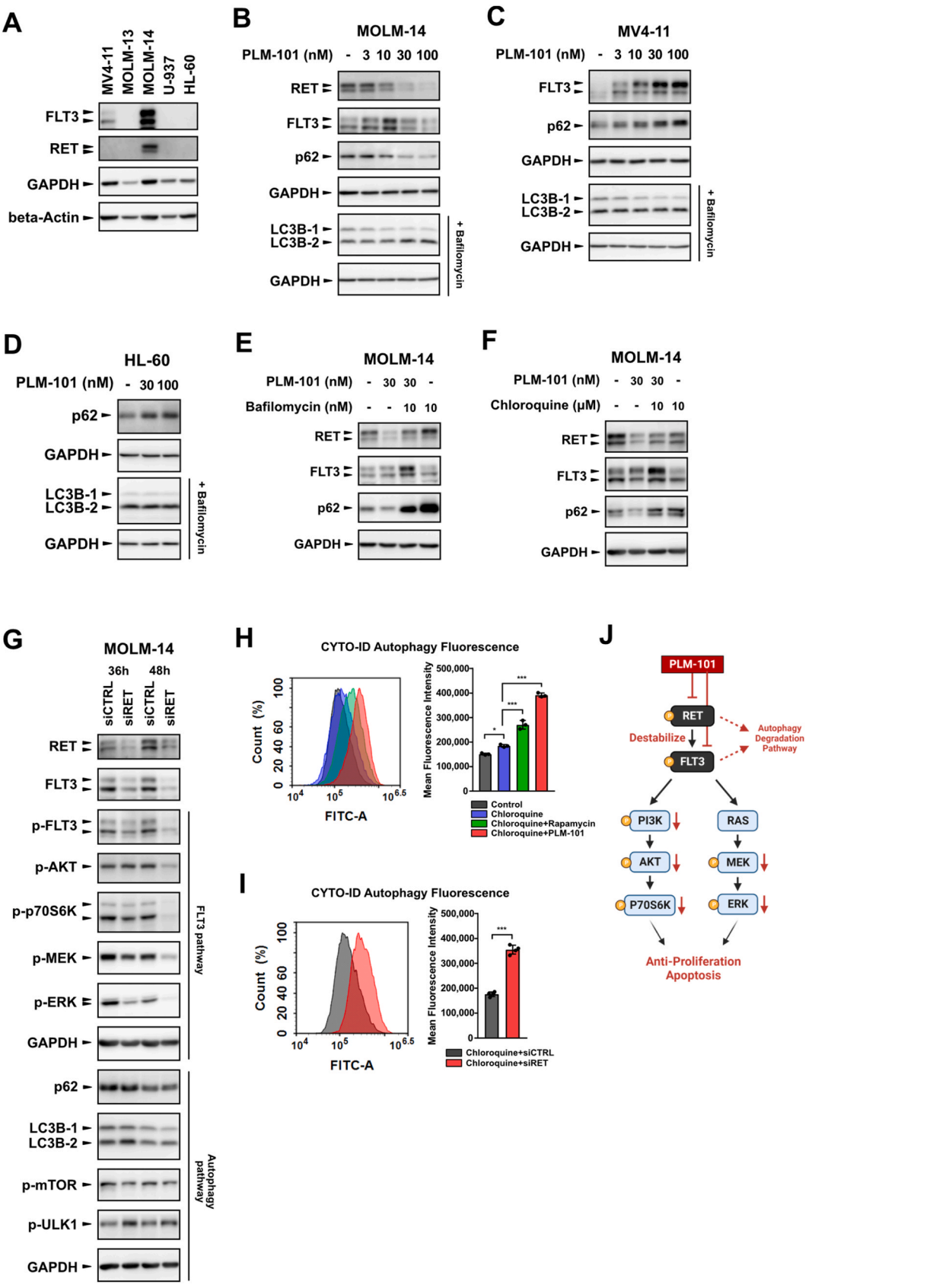

(caption on next page)

Fig. 4. The inhibition of RET has an impact on the stability of FLT3-ITD protein through the regulation of autophagy. (A) The basal expression level of FLT3 and RET protein. (B) The impact of PLM-101 on the levels of RET, FLT3 protein, as well as the induction of autophagy markers in RET-positive AML cell line (MOLM-14). The LC3B protein was detected under 10 nM Bafilomycin treatment. (C, D) The impact of PLM-101 on the levels of FLT3 protein, as well as the changes of autophagy markers in RET negative AML cell line (MV4–11 and HL-60). The LC3B protein was detected under 10 nM Bafilomycin treatment. (E, F) Restoration of RET and FLT3 protein degradation by co-treatment with Bafilomycin or Chloroquine. Bafilomycin and Chloroquine concentration used are 10 nM or 10 μM, respectively. In figure B-F, PLM-101 was treated for 24 h at the indicated concentration. (G) Changes in autophagy and FLT3 sub-activation pathways by RET knockdown. RET specific knockdown was performed for 36 and 48 h. (H) Confirmation of autophagosome accumulation by PLM-101 treatment using CYTO-ID autophagy detection kit. Experiment was performed under 10 μM Chloroquine. According to the protocol, rapamycin 0.5 μM was used as a positive control (I) Confirmation of autophagosome accumulation by RET knockdown using CYTO-ID autophagy detection kit. Experiment was performed under 10 μM Chloroquine. (J) Schematic illustration of RET/FLT3 dual target mechanism. All data represent the mean ± SD. Statistical significance of the differences in Fig. H was determined by one-way ANOVA followed by the Tukey's test. Statistical significance of the differences in Fig. I was determined by unpaired two-tailed Student t-test. * , $P < 0.05$, * *, $P < 0.01$, * ** , $P < 0.001$.

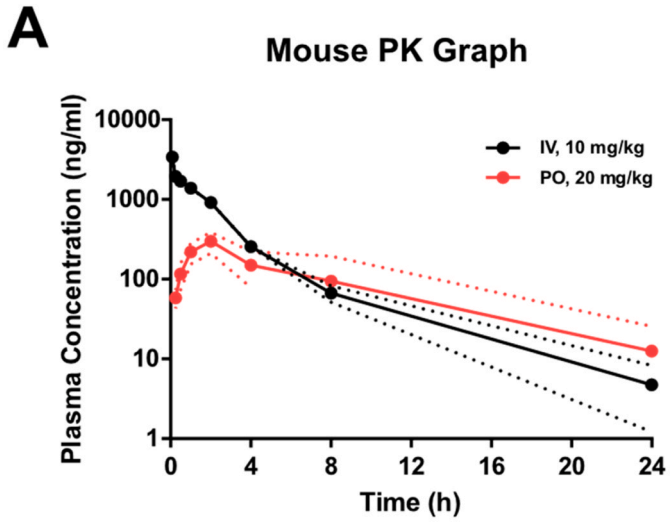

Table 3 Mouse PK Summary

Parameter	IV, 10 mg/kg	Parameter	PO, 20 mg/kg
C_0 (ng/mL)	4,483 ± 426	Bioavailability (%)	17.6
$T_{1/2}$ (h)	3.60 ± 0.797	C_{max} (ng/mL)	299 ± 87.5
Vd_{ss} (L/kg)	5.41 ± 1.08	T_{max} (h)	2.00
CL (mL/min/kg)	32.7 ± 1.37	$T_{1/2}$ (h)	5.44 ± 2.87
T_{last} (h)	24.0 ± N/D	T_{last} (h)	24.0 ± N/D
$AUC_{0\text{-last}}$ (ng·h/mL)	5,071 ± 231	$AUC_{0\text{-last}}$ (ng·h/mL)	1,788 ± 471
$AUC_{0\text{-inf}}$ (ng·h/mL)	5,099 ± 205	$AUC_{0\text{-inf}}$ (ng·h/mL)	1,919 ± 566
$MRT_{0\text{-last}}$ (h)	2.60 ± 0.292	$MRT_{0\text{-last}}$ (h)	6.15 ± 0.548
$MRT_{0\text{-inf}}$ (h)	2.75 ± 0.429	$MRT_{0\text{-inf}}$ (h)	7.92 ± 1.80
AUC_{Extra} (%)	0.550 ± 0.540	AUC_{Extra} (%)	6.27 ± 6.06
$AUMC_{Extra}$ (%)	5.52 ± 4.81	$AUMC_{Extra}$ (%)	24.4 ± 21.8

Fig. 5. The examination of pharmacokinetic profile of PLM-101 in mice. (A) Changes in plasma concentration of drugs over time after single administration. The mice used were 7–9 week-old male ICR mice. N = 3. All data represent the mean ± SD.

Table 3
Summary of various pharmacokinetic properties.

Parameter	IV, 10 mg/kg	Parameter	PO, 20 mg/kg
C_0 (ng/mL)	4483 ± 426	**Bioavailability (%)**	17.6
$T_{1/2}$ (h)	3.60 ± 0.797	**C_{max} (ng/mL)**	299 ± 87.5
Vd_{ss} (L/kg)	5.41 ± 1.08	**T_{max} (h)**	2.00
CL (mL/min/kg)	32.7 ± 1.37	**$T_{1/2}$ (h)**	5.44 ± 2.87
T_{last} (h)	24.0 ± ND	**T_{last} (h)**	24.0 ± ND
$AUC_{0\text{-last}}$ (ng·h/mL)	5071 ± 231	**$AUC_{0\text{-last}}$ (ng·h/mL)**	1788 ± 471
$AUC_{0\text{-inf}}$ (ng·h/mL)	5099 ± 205	**$AUC_{0\text{-inf}}$ (ng·h/mL)**	1919 ± 566
$MRT_{0\text{-last}}$ (h)	2.60 ± 0.292	**$MRT_{0\text{-last}}$ (h)**	6.15 ± 0.548
$MRT_{0\text{-inf}}$ (h)	2.75 ± 0.429	**$MRT_{0\text{-inf}}$ (h)**	7.92 ± 1.80
AUC_{Extra} (%)	0.550 ± 0.540	**AUC_{Extra} (%)**	6.27 ± 6.06
$AUMC_{Extra}$ (%)	5.52 ± 4.81	**$AUMC_{Extra}$ (%)**	24.4 ± 21.8

All data represent the mean ± SD. ND: not determined.

knockdown of *RET* by siRNA also led to an increase in autophagy markers, including decreases in p62 and phospho-S2448 mTOR, and increases in LC3B-2/LC3B-1 ratio and phospho-S555 ULK1 (Fig. 4 G). Additionally, a decrease in the activation of FLT3 sub-pathways, including the PI3K and Ras signaling pathways, was observed (Fig. 4G). However, a decrease in phospho-S555-ULK1 also was observed by PLM-101 treatment, which likely was due to the drug's multi-kinase inhibitory effects (Fig. S2E). Furthermore, both PLM-101 treatment and knockdown of *RET* led to an increase in autophagy, resulting in the accumulation of autophagosomes (Fig. 4H, I). Collectively, these results demonstrate that RET-targeting by PLM-101 activates the autophagy degradation pathway, leading to degradation of both RET and FLT3, and additional inhibition of FLT3 sub-pathway activation (Fig. 4 J).

3.5. Pharmacokinetic profile of PLM-101 in mice

Currently, there are two U.S. FDA-approved drugs, Midostaurin and Gilteritinib, for treatment of relapsed/refractory FLT3-mutated AML patients in oral dosage form. Therefore, to evaluate the feasibility of PLM-101 as an oral formulation, its *in vivo* pharmacokinetic properties were determined. The time-course of the plasma concentration of PLM-101 after intravenous (IV) and Oral (PO) administration is depicted in Fig. 5A. Although the oral bioavailability of PLM-101 is approximately 17.6%, which is relatively lower than that of Gilteritinib [44], it was still deemed useful as an oral formulation. Additional pharmacokinetic properties are presented in Table 3.

3.6. Anti-leukemic effect of PLM-101 on in vivo flank xenograft model

To evaluate the preclinical anti-leukemic activity of PLM-101, AML cells were implanted into the flank of BALB/C nude mice, and PLM-101 was orally administered once per day (Fig. 6 A). The results of flank xenograft experiments using two types of AML cell lines demonstrated a promising anti-cancer efficacy of PLM-101 (Figs. 6B, D, S3A), with no observed change in body weight during the administration period (Fig. 6C, E). To confirm whether the mechanism identified in the cell-based experiments would also appear in the animal models, AML cells were transplanted into the flank of BALB/C nude mice, and PLM-101 was orally administered for 5 days, after which tumor tissues were collected. The tumor tissues treated with PLM-101 showed similar outcomes to the cell experiments, with suppression of the FLT3 downstream pathways and an increase in markers of apoptosis, including elevated levels of the cleaved forms of caspase-3 and PARP, as well as an increased TUNEL-stained area (Fig. 6F, G). Moreover, in the tumor tissues from a MOLM-14 flank xenograft model, protein degradation of RET and FLT3, and activation of autophagy markers (decrease in p62 and increase in LC3B-2/LC3B-1 ratio) were detected, similarly to the *in vitro* experiments (Fig. 6H, I).

3.7. Anti-leukemic effect of PLM-101 on in vivo orthotopic xenograft model

The placement of tumors in their original anatomical location (orthotopic implantation) offers a more accurate representation of their behavior and of anti-cancer drug activity [45,46]. To evaluate the anti-leukemic activity of PLM-101 in an orthotopic model, luciferase-overexpressing AML cells were injected into the tail vein of NSGA mice (Fig. 7A). Oral administration of PLM-101 showed a significant decrease in leukemia growth as quantified by *in vivo* fluorescence in the mice, and significantly improved their survival rate. The median survival for the control group was 18 days, whereas for the groups treated with 3, 10, and 20 mg/kg of PLM-101, it was 23, 35 days and undefined, respectively (Fig. 7B-7E). Various studies employing AML orthotopic xenograft experimentation have confirmed that AML cells can spread and grow in the bone marrow, spleen, and liver [47,48]. Correspondingly, we detected MV4–11-luc cells in bone marrow, spleen, and liver (Fig. S3B). Next, to verify that the autophagy mechanism was also induced in the orthotopic xenograft model, MOLM-14-luc cells were injected into the tail vein and treated with PLM-101 for 14 days. The distribution of AML cells in the bone marrow, spleen, and liver was measured using flow cytometry, as illustrated in Fig. 7H. Preclinical models of AML cells expressing RET also showed a significant decrease in *in vivo* fluorescence. Additionally, a reduction in the expression of RET and an accumulation of autophagosomes were observed in the bone marrow and liver of the mice (Fig. 7I-K). Overall, the results of both the flank and orthotopic xenograft models demonstrated the anti-leukemic efficacy of PLM-101 and its effected RET-mediated autophagic degradation.

3.8. Safety assessment of PLM-101

Treatment failure resulting from adverse events associated with FLT3 inhibitors, such as liver toxicity and hematologic toxicity, has highlighted the need to develop FLT3-targeting drugs of reduced toxicity [22–24]. In the current study, to determine the potential side effects and toxicity of PLM-101, both *in vitro* and *in vivo* experiments were performed. Among the mice, even with a single dose of 2000 mg/kg, which is 100 times higher than the effective dose in xenograft models (Table 4), no death occurred. Furthermore, no significant adverse effects related to hepatotoxicity or hematologic toxicity were observed, even after repeated daily administration of doses at 40, 80, and 160 mg/kg for 2 weeks, which were higher than the effective dose in the xenograft models (Table 5, Table 6). Nonetheless, a decline in normal monocytes was observed (Table 5), which was likely due to the impact of FLT3 on the proliferation and differentiation of monocytes [11]. Based on the results, it was verified that the no observed adverse effect level (NOAEL) of PLM-101 was over 160 mg/kg/day. More detailed information relating to Tables 5 and 6 can be found in Tables S3 and S4, respectively. The plasma protein binding of PLM-101 was 97.61% for mouse proteins and 99.01% for human proteins (Table S2). The inhibition of different CYP enzymes by PLM-101 was found to be relatively low, except for CYP 1A2 (Table S1), indicating the relatively low drug interaction of PLM-101. Overall, it was verified that PLM-101, with its minimal toxicity at effective therapeutic doses, could be a safe anti-cancer agent.

3.9. pH-dependent solubility and saturated absorption of PLM-101 in gastrointestinal tract

PLM-101 exhibited a maximum solubility of 2.0 mg/mL in water only under the gastric acid condition (pH 1.2), whereas it was almost insoluble in water at pH above 7.0 (Table 7). Furthermore, its solubility was tested using a buffer that simulates the following gastric and intestinal fluids: simulated gastric fluid (SGF), fed-state simulated intestinal fluid (FeSSIF), and fasted-state simulated intestinal fluid (FaSSIF). PLM-101 showed a maximum solubility of approximately 2.0 mg/mL in

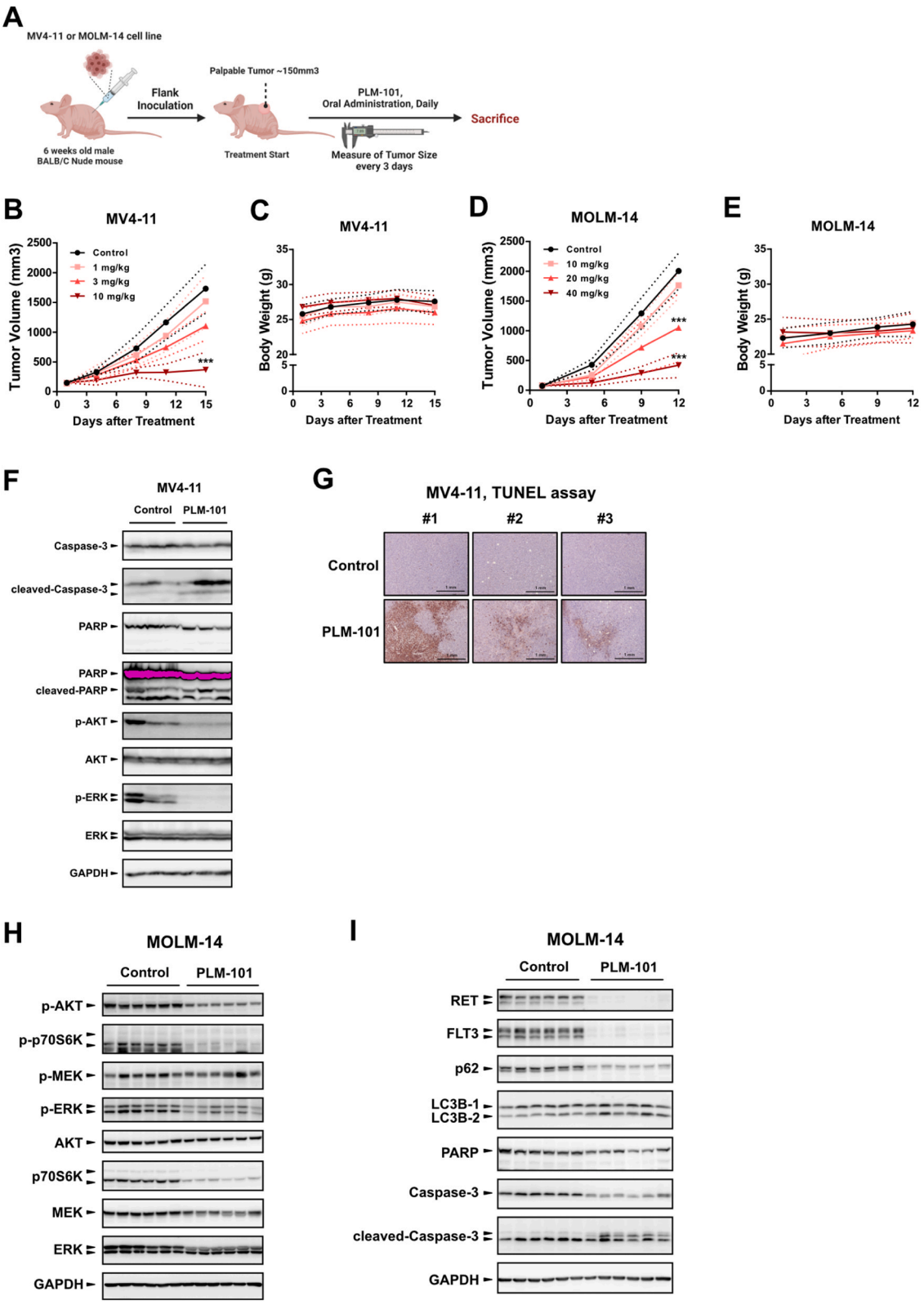

Fig. 6. The evaluation of anti-leukemic efficacy using in vivo flank xenograft model. (A) Schematic illustration of in vivo flank xenograft model. The mice used were 6-week-old male BALB/c-nu mice. After the tumor had grown to a volume of 100–150 mm^3, PLM-101 was administered orally on a daily basis. Tumor volume and body weight were measured twice a week. (B) Efficacy of PLM-101 in MV4–11 flank xenograft model. N = 6. (C) Changes in body weight in MV4–11 flank xenograft model. N = 6. (D) Efficacy of PLM-101 in MOLM-14 flank xenograft model. N = 6. (E) Changes in body weight in MOLM-14 flank xenograft model. N = 6. (F) Changes in apoptosis markers and FLT3 sub-activation pathway, (G) TUNEL stained area were detected in MV4–11 flank xenograft tumor tissue. 20 mg/kg PLM-101 were administered for 5 days. N = 3. (H) Changes in FLT3 sub-activation pathway, and (I) autophagy markers, RET, and FLT3 protein expression using western blotting in MOLM-14 flank xenograft tumor tissue. 80 mg/kg PLM-101 were administered for 5 days. N = 6. All data represent the mean ± SD. Statistical significance of the differences in all figures was determined by one-way ANOVA followed by the Tukey's test. * ** , $P < 0.001$.

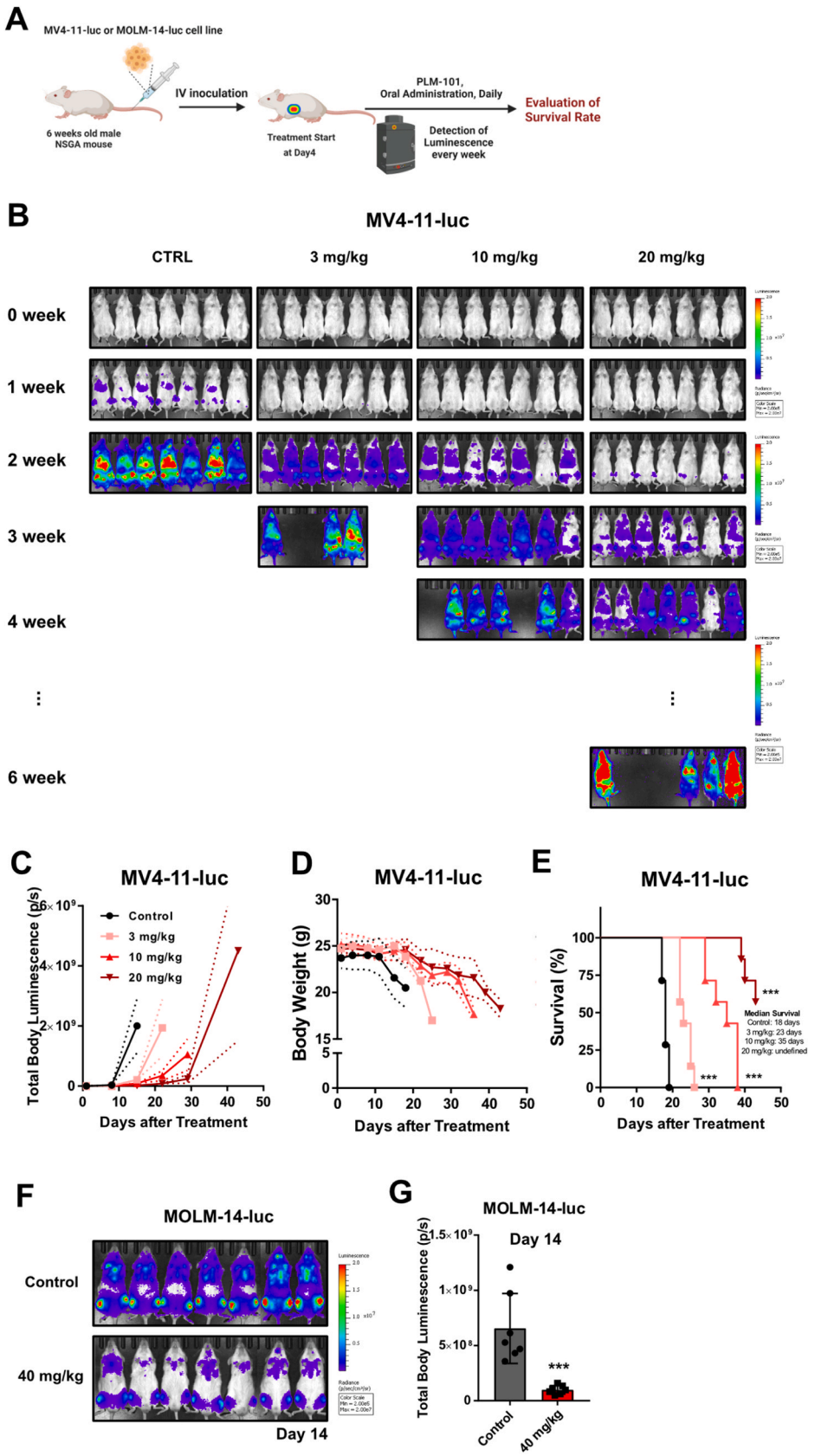

Fig. 7. The evaluation of anti-leukemic efficacy using in vivo orthotopic xenograft model. (A) Schematic illustration of in vivo orthotopic xenograft model. The mice were used 6-week-old male NSGA (NOD/ShiLtJ-Prkdc^{em1AMC}Il2rg^{em1AMC}) mice. 4 days after tail vein injection of AML cells, PLM-101 was administered orally on a daily basis. Bioluminescence was detected once a week and body weight were measured twice a week. 150 mg/kg luciferin were treated 10 min before bioluminescence detection. (B) The picture of bioluminescence, (C) total body luminescence (photons/sec), (D) body weights, (E) survival rate in MV4–11-luc orthotopic xenograft model. N = 7. The experiment was terminated on day 43. The median survival values were control: 18 days, 3 mg/kg: 23 days, 10 mg/kg: 35 days, 20 mg/

kg: undefined. (F) The picture of bioluminescence, (G) total body luminescence (photons/sec) in MOLM-14-luc orthotopic xenograft model. N = 7. The experiment was terminated on day 14. (H) Schematic illustration of immune cell population collection from liver, bone marrow, and spleen. In flow cytometry analysis. Main immune cell population were gated by FSC-A/SSC-A. Single cell population were gated by FSC-A/FSC-H. Human AML cell (MOLM-14-luc) were gated by human CD45-positive population. Human RET expression was detected in hCD45-positive population. Autophagosome was detected in hRET/hCD45 double-positive population. (I) Infiltrated hCD45-positive cells, hRET MFI and autophagosome MFI in bone marrow, (J) in liver, (K) in spleen from MOLM-14-luc orthotopic xenograft model. All data represent the mean ± SD. Statistical significance of the differences in all figures was determined by one-way ANOVA followed by the Tukey's test. * , $P < 0.05$, * *, $P < 0.01$, * ** , $P < 0.001$.

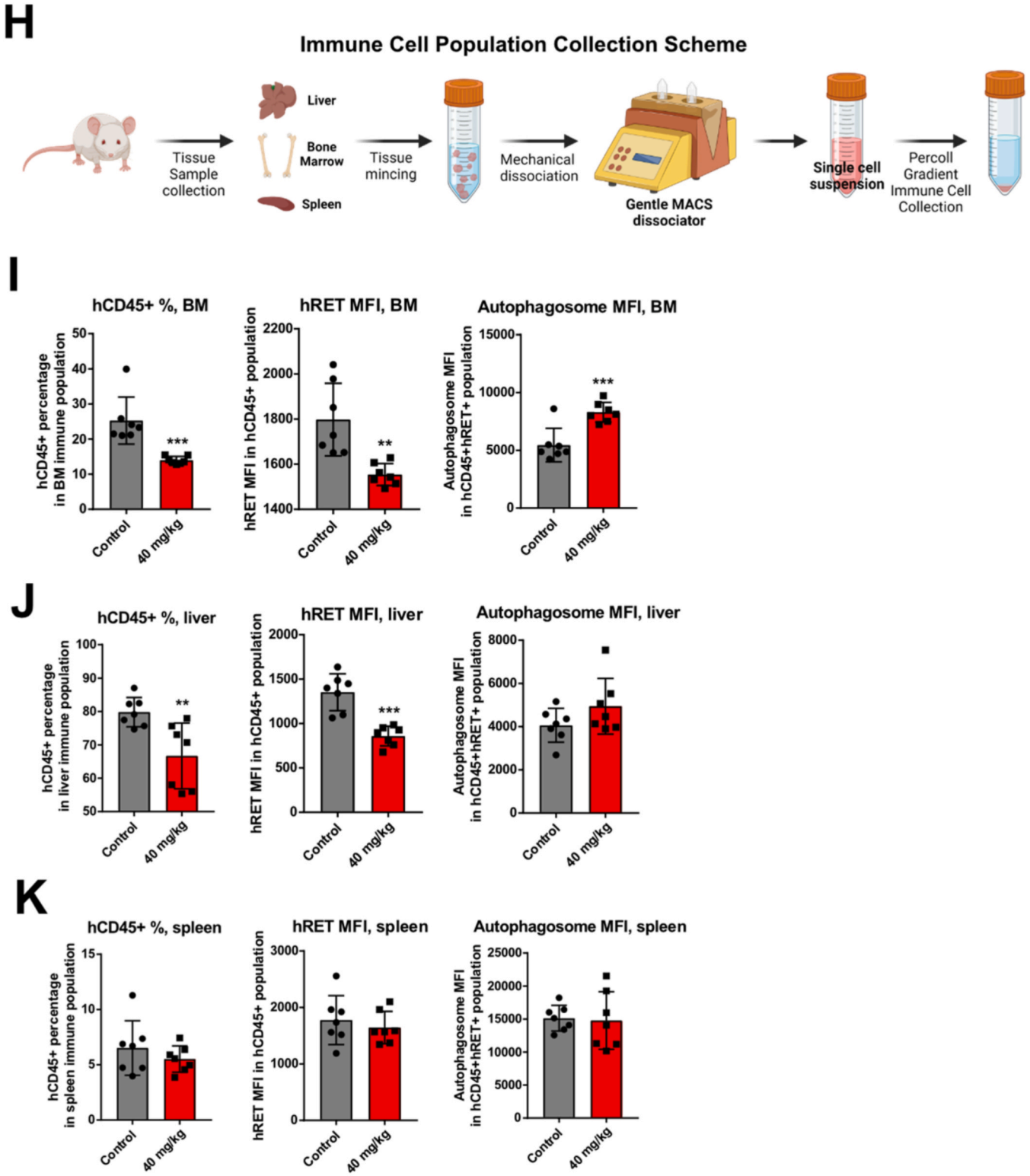

Fig. 7. (*continued*).

Table 4
Single-dose toxicity test of PLM-101.

Dose (mg/kg)	Unscheduled Death
Vehicle	0/10
222.2	0/10
666.7	0/10
2000	0/10

The drug was administered orally at the indicated dose. 7-week-old male ICR mice were used. N = 10.

Table 5
Repeated-dose toxicity test of PLM-101. The hematological parameters.

Parameter	Vehicle	40 mg/kg	80 mg/kg	160 mg/kg
WBC	3.15 ± 0.70	3.80 ± 1.29	3.00 ± 1.10	3.90 ± 0.60
RBC	8.38 ± 0.46	7.90 ± 0.95	7.38 ± 1.08	8.36 ± 0.53
HGB	13.86 ± 0.51	12.92 ± 0.56	12.46 ± 0.72	13.43 ± 0.59
HCT	45.01 ± 2.40	42.72 ± 2.24	42.02 ± 1.92	44.21 ± 2.10
MCV	53.73 ± 1.21	52.92 ± 2.30	52.80 ± 3.25	52.97 ± 1.77
MCH	16.52 ± 0.58	15.92 ± 0.35	15.85 ± 0.71	16.00 ± 0.49
MCHC	30.79 ± 1.18	30.12 ± 1.24	30.43 ± 1.06	30.37 ± 0.89
RDW	12.68 ± 0.73	12.63 ± 0.68	12.91 ± 0.94	12.80 ± 0.63
HDW*	1.94 ± 0.16	1.91 ± 0.15	2.11 ± 0.13	2.18 ± 0.14
PLT	1151.8 ± 181.6	1132.4 ± 172.2	1159.2 ± 219.0	1215.6 ± 133.3
MPV	5.96 ± 0.31	6.04 ± 0.47	6.15 ± 0.39	6.11 ± 0.34
NEUT	23.24 ± 7.72	24.82 ± 9.36	24.70 ± 7.66	26.01 ± 5.56
LYM	71.39 ± 7.98	70.19 ± 8.95	71.02 ± 7.53	71.13 ± 5.62
MONO* *	1.54 ± 0.76	1.17 ± 0.51	0.67 ± 0.39	0.57 ± 0.35
EOS	2.66 ± 1.35	2.39 ± 0.97	2.42 ± 1.77	1.27 ± 1.05
LUC	0.94 ± 0.37	1.19 ± 0.87	0.98 ± 0.63	0.84 ± 0.71
BASO	0.31 ± 0.17	0.27 ± 0.22	0.23 ± 0.12	0.26 ± 0.15
Retic*	3.82 ± 0.65	4.31 ± 0.99	4.66 ± 0.87	5.04 ± 0.82

The drug was administered orally at the indicated dose for 2-week. 7-week-old male ICR mice were used. N = 10. All data represent the mean ± SD. Statistical significance of the differences in Table 5 was determined by one-way ANOVA followed by the Tukey's test. Only statistical data for the vehicle and 160 mg/kg group are shown. * , $P < 0.05$, * *, $P < 0.01$, * ** , $P < 0.001$.

SGF at pH 2.0, but did not dissolve in either FeSSIF at pH 5.0 or FaSSIF at pH 6.5 (Table 7), demonstrating that its solubility is highly sensitive to pH. To determine whether the low toxicity of PLM-101 was due to limited absorption caused by changes in solubility or limited maximum solubility, the plasma drug concentration was monitored post-administration in mice for 7 or 14 days. Even after high-dose administration, there was no significant change in the plasma drug concentration, and neither was there any significant alteration in the plasma drug concentration between the 7-day and 14-day administrations, at any dose (Fig. 8 A). When pretreated with Metoclopramide and Famotidine to induce increased gastric emptying and gastric pH, a trend towards reduced drug absorption was observed (*P* value=0.091) (Fig. 8B). Hence, it seems possible that the low toxicity of PLM-101 may be due to saturated and limited absorption at high doses, as it is soluble and absorbed only in the stomach (Fig. 8 C).

4. Discussion

The significance of *FLT3* mutations in AML has been highlighted in recent studies. The mutant form of FLT3 promotes the growth of AML cells through the hyperactivity of its kinase pathway [11–14]. Breakthroughs have been made in the development of drugs targeting FLT3, two FLT3-targeting drugs having been approved by U.S. FDA for treatment of AML patients with *FLT3* mutations [49]. However, acquired-resistant mutations such as D835Y or F691L in the FLT3-tyrosine kinase domain, which arise during FLT3-targeting therapy, have been shown to reduce the anti-leukemic efficacy of these types of agents [10,20]. In addition, the hepatotoxicity, hematological toxicity, and cardiotoxicity of these drugs have been pointed out as possible causes of treatment failure [22,50].

Traditional Chinese medicine (TCM), which has been practiced for centuries, and is now commonly recognized as an alternative form of cancer treatment [51]. TCM possesses several unique features, including its multi-targeting ability, its minimal side effects, and its potent therapeutic outcomes [52]. These effects are attributed to either the powerful anti-cancer properties of its active components, or some combination of them. Consequently, several TCMs and their active components recently have been introduced as useful treatment modalities for anti-cancer therapy [51,52]. Indirubin, a bisindole alkaloid substance, is the principal bioactive component of *Indigo naturalis*, and is also present in other traditional Chinese medicines such as *Radix Isatidis*

Table 7
Maximum solubility of PLM-101 by pH value.

PLM-101	pH 1.2	pH 7.4	SGF (pH 2.0)	FeSSIF-v1 (pH 5.0)	FaSSIF-v1 (pH 6.5)
Solubility (mg/mL), 2 h	1.8	0.001	1.7	0.2	0.02
Solubility (mg/mL), 24 h	> 2.0	0.001	1.9	0.2	0.03

SGF: simulated gastric fluid. FeSSIF: fed-state stimulated intestinal fluid. FaSSIF: fasted-state stimulated intestinal fluid.

Table 6
Repeated-dose toxicity test of PLM-101. The histopathological parameters.

Parameter	Vehicle	40 mg/kg	80 mg/kg	160 mg/kg
Albumin	2.02 ± 0.09	1.90 ± 0.10	1.90 ± 0.10	1.90 ± 0.00
ALP	355.92 ± 88.35	290.62 ± 70.63	270.96 ± 115.09	333.08 ± 85.16
ALT(GPT)	34.52 ± 8.38	28.90 ± 11.63	31.10 ± 8.89	33.17 ± 8.75
AST(GOT)	109.89 ± 22.03	78.92 ± 15.52	110.22 ± 35.47	106.86 ± 37.89
T. Bil	0.17 ± 0.02	0.17 ± 0.03	0.15 ± 0.03	0.16 ± 0.04
BUN	23.28 ± 4.56	23.20 ± 7.54	23.01 ± 7.09	23.35 ± 8.40
Ca	9.75 ± 0.38	9.43 ± 0.46	9.21 ± 0.54	9.30 ± 0.24
T. Cholesterol	112.23 ± 22.61	108.38 ± 26.32	104.33 ± 32.33	101.69 ± 9.09
CK(CPK)	187.26 ± 51.22	117.35 ± 45.94	192.99 ± 79.38	187.91 ± 72.22
Creatinine	0.26 ± 0.05	0.23 ± 0.04	0.23 ± 0.05	0.22 ± 0.03
Glucose	122.06 ± 28.16	133.13 ± 14.50	134.66 ± 36.71	139.59 ± 32.68
PI	9.13 ± 0.87	8.95 ± 1.07	9.82 ± 0.85	9.71 ± 0.58
Total Protein	4.97 ± 0.23	4.75 ± 0.28	4.44 ± 0.40	4.72 ± 0.23
TG	33.37 ± 12.44	34.22 ± 12.43	30.87 ± 9.00	29.58 ± 16.69
A/G ratio	0.67 ± 0.03	0.67 ± 0.04	0.65 ± 0.05	0.67 ± 0.03
Na	149.50 ± 1.27	149.20 ± 2.04	149.20 ± 3.12	149.90 ± 1.91
K	6.67 ± 0.81	6.54 ± 0.61	6.46 ± 0.80	6.84 ± 0.53
Cl	115.80 ± 1.40	115.60 ± 2.22	116.50 ± 2.07	116.00 ± 1.49

The drug was administered orally at the indicated dose for 2-week. 7-week-old male ICR mice were used. N = 10. All data represent the mean ± SD.

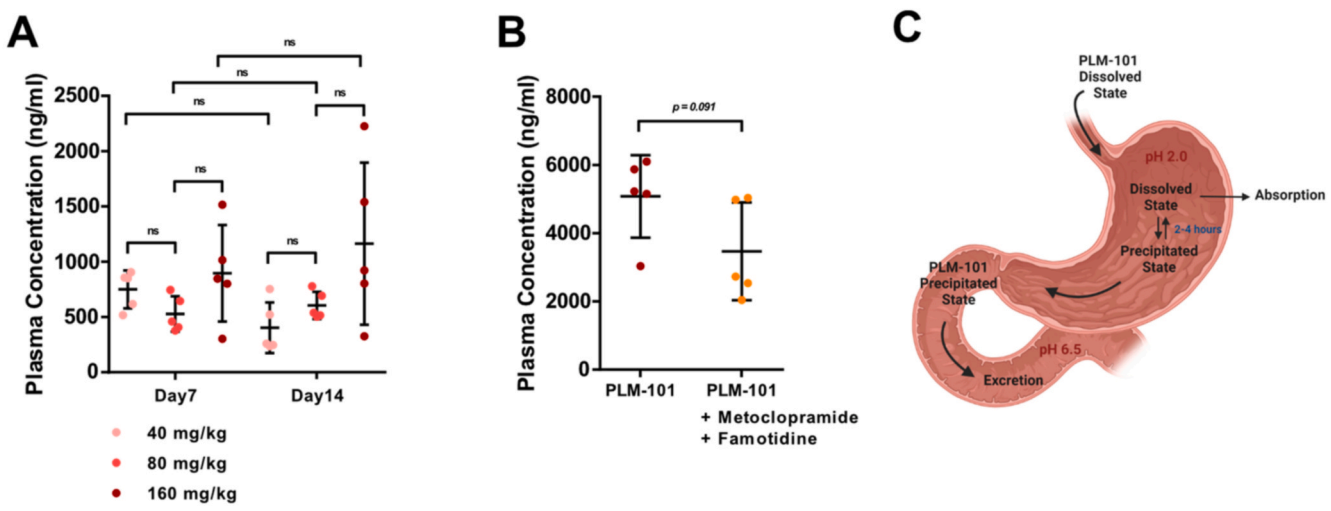

Table 7

PLM-101	pH 1.2	pH 7.4	SGF (pH 2.0)	FeSSIF-v1 (pH 5.0)	FaSSIF-v1 (pH 6.5)
Solubility (mg/ml), 2h	1.8	0.001	1.7	0.2	0.02
Solubility (mg/ml), 24h	> 2.0	0.001	1.9	0.2	0.03

Fig. 8. The limited absorption of PLM-101, which is dependent on pH and maximum solubility, is responsible for its low toxicity. (A) Detection of plasma concentration of PLM-101 through repeated administration. C57BL/6 J mice were administered for 7 days and 14 days. Plasma concentrations of the drug were measured 4 h after administration. N = 5. (B) Restoration of PLM-101 absorption by pretreatment with Metoclopramide and Famotidine. C57BL/6 J mice were fasted for 12 h. Metoclopramide and Famotidine have been used to induce increased gastric emptying rate and gastric pH, respectively. 10 mg/kg Metoclopramide and 10 mg/kg Famotidine injected by intraperitoneally (IP) 30 min before and subsequently 160 mg/kg PLM-101 administered by oral gavage (PO). Plasma concentrations of the drug were measured 2 h after PLM-101 administration. N = 5. (C) Schematic illustration of the absorption process at the stomach. All data represent the mean ± SD. Statistical significance of the differences in Fig. A was determined by one-way ANOVA followed by the Tukey's test. Statistical significance of the differences in Fig. B was determined by unpaired two-tailed Student t-test. ns: no significant, $p > 0.05$.

and *Folium Isatidis* [53]. Despite its low water solubility and bioavailability, indirubin exhibits low toxicity and has been demonstrated to possess anti-cancer, anti-bacterial, and anti-inflammatory properties. Consequently, there have been sustained endeavors to employ indirubin derivatives as anti-cancer agents [53–55]. Here, we present PLM-101 as a new FLT3 inhibitor that can overcome the problems of current FLT3-targeting therapy. In the present study, PLM-101 as an indirubin derivative improved the insoluble property of indirubin. It also demonstrated superior *in vitro* anti-leukemic activities in FLT3-mutant AML cells to those of Gilteritinib, an U.S. FDA-approved FLT3-targeting drug (Table 2). Furthermore, various toxicity tests demonstrated the high safety of PLM-101 in terms of low incidences of liver toxicity and hematological toxicity (Tables 4–6).

Clinical trials have revealed that FLT3 inhibitors cause development of resistance among some patients [10]. This resistance is mainly due to a secondary mechanism that counteracts the FLT3 inhibitors' actions and is classified into two categories: on-target and off-target resistance [10]. Leukemia cells in cases of on-target resistance continue to rely on FLT3 activity but acquire resistance to FLT3 inhibitors through additional mutations in the *FLT3* gene. Conversely, off-target resistance is caused by mutations in genes other than the *FLT3* gene, such as *KRAS, NRAS, BRAF, IDH2, CEBPA* and *RUNX1* [10]. In the study, we found that PLM-101 effectively suppressed the proliferation of Ba/F3 cells expressing on-target resistance mutations D835Y and F691L (Table 1). Additionally, it was also confirmed that FLT3 downstream signaling pathway was effectively reduced by PLM-101 in these cells (Fig. S4). Of particular note, the F691L mutation, which is a type of on-target resistance mutation, confers resistance to various FLT3-targeting agents such as Gilteritinib, Midostaurin, Quizartinib, Sorafenib, and Crenolanib [10]. Despite a 15-fold increase in IC50 for FLT3-ITD-F691L compared to FLT3-ITD, it still maintains a 2.2-fold lower IC50 compared to Gilteritinib (Table 1). Therefore, the ability of PLM-101 to inhibit FLT3-ITD-F691L at a lower concentration compared to Gilteritinib can be inferred, making it a superior alternative to Gilteritinib and a potential treatment option for secondary mutations. However, considering the limited *in vivo* efficacy of PLM-101 in MOLM-14 xenograft study and the saturated plasma concentration after oral administration, the clinical application of PLM-101 against FLT3-ITD-F691 would be limited.

Recently, the role of autophagy in the degradation process of FLT3 has been extensively examined [32–35]. One study showed that activation of RET promotes the proliferation of AML cells by stabilizing FLT3 protein [31]. In that study, a combination of FLT3 inhibitor Crenolanib with RET inhibitors such as Vandetanib or Danusertib, significantly reduced the proliferation and viability of FLT3-ITD mutant AML cells [31]. Thus, targeting of RET can effectively block FLT3-dependent AML cell growth by promoting FLT3 protein degradation. However, there are currently no drugs available that target both FLT3 and RET simultaneously. Here, in the current study, we confirmed that *RET* knockdown promotes the degradation of FLT3 through activation of the autophagy pathway (Fig. 4 G, 4I). Furthermore, we confirmed the protein degradation of RET and FLT3 through the activation of autophagy by PLM-101 (Fig. 4). In a short-term experiment (Table 2), the anti-leukemic activity of PLM-101 (a FLT3/RET dual-targeting therapy) was found to be only marginally superior to that of Gilteritinib. Nevertheless, in the context of an extended clinical treatment regimen including multiple cycles, targeting of RET in

addition to FLT3 may result in more potent anti-leukemic efficacy due to the degradation of FLT3.

The flank xenograft model has served as a valuable research tool for assessing anti-cancer efficacy since 1969 [56,57]. However, its utility in reflecting the actual environment in which cancer grows is limited [58]. Consequently, in this study, we employed an orthotopic xenograft model to more accurately evaluate the anti-leukemic efficacy of PLM-101 and replicate the clinical setting of AML. Orthotopic implantation involves placing tumors at the identical site where the primary cancer developed in the patient, based on Paget's principle that a tumor will flourish better in a familiar and suitable environment [59,60]. Although the experimental dose failed to achieve complete remission of AML in the orthotopic xenograft model, it resulted in a noteworthy enhancement in mice survival (as shown in Fig. 7A-7 G). The reduced anti-leukemic efficacy observed in the orthotopic xenograft model (Fig. 7), relative to that in the flank xenograft model (Fig. 6) could be attributed to factors such as the impact of the tumor microenvironment or the distribution of drugs to organs. Additionally, we observed the activation of autophagy *via* RET inhibition and subsequent degradation of its protein in AML cells that had metastasized to the bone marrow and liver (Figs. 7I, 7 J).

Another important point to note regarding this study is that repeated administration of PLM-101 did not cause any significant increase in plasma drug concentration (Fig. 8 A). This may have been due to the limited solubility of PLM-101 in the small-intestine environment (Table 7). In terms of drug absorption, it is worth noting that while most drugs are primarily absorbed in the small intestine [61], PLM-101 exhibits high solubility only in gastric acid with low pH. Therefore, it is expected that absorption in the small intestine will be negligible for PLM-101. PLM-101 dissolves and is absorbed at the maximum solubility within 2–4 h in the stomach, and any remaining unabsorbed amount precipitates to the duodenum and can be excreted (Fig. 8 C). Indeed, pre-treatment with Metoclopramide and Famotidine, which increase the gastric emptying rate and gastric pH, respectively, led to reduced PLM-101 absorption (Fig. 8B). Despite the limited absorption in the small intestine, if the blood saturation concentration of PLM-101 exceeds the concentration required to elicit anti-leukemia effects during repeated administration, it could be advantageous in reducing differential adverse effects arising from differences among individual clinics.

In summary, this study confirmed that the RET-mediated autophagy degradation pathway regulates the stabilization of FLT3 protein. In addition, this study has revealed a novel drug showing the potential for clinical application in targeting both FLT3 and RET. Moreover, in view of the results of this investigation and of other, similar studies, it is anticipated that indirubin and its derivatives will serve as efficacious anti-AML agents.

CRediT authorship contribution statement

Yong June Choi: Conceptualization, Methodology, Validation, Formal analysis, Investigation, Writing – original draft, Writing – review & editing, Visualization. **Jaewoo Park**: Investigation. **Hyoyi Choi**: Investigation. **Su-Jin Oh**: Investigation. **Jin-Hee Park**: Investigation. **Miso Park**: Investigation. **Ji Won Kim**: Investigation. **Yoon-Gyoon Kim**: Investigation. **Yong-Chul Kim**: Resources, Supervision. **Myung Jin Kim**: Resources, Supervision, Funding acquisition. **Keon Wook Kang**: Conceptualization, Resources, Writing – original draft, Writing – review & editing, Project administration, Supervision, Funding acquisition.

Declaration of Competing Interest

The authors declare the following financial interests/personal relationships which may be considered as potential competing interests: Keon Wook Kang reports a relationship with PeleMed that includes: equity or stocks. Myung Jin Kim reports a relationship with PeleMed that includes: board membership and equity or stocks. Yong-Chul Kim reports a relationship with PeleMed that includes: board membership and equity or stocks. Su-Jin Oh reports a relationship with PeleMed that includes: employment. Jin-Hee Park reports a relationship with PeleMed that includes: employment. SJ Oh, JH Park, YC Kim and MJ Kim are working at Pelemed.

Data availability

Data will be made available on request.

Acknowledgement

This research was supported by a grant of the Korea Health Technology R&D Project through the Korea Health Industry Development Institute (KHIDI), funded by the Ministry of Health & Welfare, Republic of Korea (Grant Number: HI21C1404) and the Technological Innovation R&D Program (Grant Number: S3029658) funded by Ministry of SMEs and Startups (MSS, Korea). All graphical figures were created using BioRender.com (BioRender, Toronto, Canada).

Appendix A. Supporting information

Supplementary data associated with this article can be found in the online version at doi:10.1016/j.biopha.2023.115066.

References

[1] F. Ferrara, C.A. Schiffer, Acute myeloid leukaemia in adults, Lancet 381 (9865) (2013) 484–495, https://doi.org/10.1016/S0140-6736(12)61727-9.
[2] I. De Kouchkovsky, M. Abdul-Hay, 'Acute myeloid leukemia: a comprehensive review and 2016 update', Blood Cancer J. 6 (7) (2016), e441 https://doi.org/10.1038/bcj.2016.50.
[3] H. Döhner, D.J. Weisdorf, C.D. Bloomfield, Acute myeloid leukemia, N. Engl. J. Med 373 (12) (2015) 1136–1152, https://doi.org/10.1056/NEJMra1406184.
[4] B. Deschler, M. Lübbert, Acute myeloid leukemia: epidemiology and etiology, Cancer 107 (9) (2006) 2099–2107, https://doi.org/10.1002/cncr.22233.
[5] H.M. Kantarjian, T.M. Kadia, C.D. DiNardo, M.A. Welch, F. Ravandi, Acute myeloid leukemia: Treatment and research outlook for 2021 and the MD Anderson approach, Cancer 127 (8) (2021) 1186–1207, https://doi.org/10.1002/cncr.33477.
[6] N. Daver, R.F. Schlenk, N.H. Russell, M.J. Levis, Targeting FLT3 mutations in AML: review of current knowledge and evidence, Leukemia 33 (2) (2019) 299–312, https://doi.org/10.1038/s41375-018-0357-9.
[7] L. Ding, T.J. Ley, D.E. Larson, C.A. Miller, D.C. Koboldt, J.S. Welch, J.K. Ritchey, M. A. Young, T. Lamprecht, M.D. McLellan, J.F. McMichael, J.W. Wallis, C. Lu, D. Shen, C.C. Harris, D.J. Dooling, R.S. Fulton, L.L. Fulton, K. Chen, H. Schmidt, J. Kalicki-Veizer, V.J. Magrini, L. Cook, S.D. McGrath, T.L. Vickery, M.C. Wendl, S. Heath, M.A. Watson, D.C. Link, M.H. Tomasson, W.D. Shannon, J.E. Payton, S. Kulkarni, P. Westervelt, M.J. Walter, T.A. Graubert, E.R. Mardis, R.K. Wilson, J. F. DiPersio, Clonal evolution in relapsed acute myeloid leukaemia revealed by whole-genome sequencing, Nature 481 (7382) (2012) 506–510, https://doi.org/10.1038/nature10738.
[8] D.A. Arber, A. Orazi, R. Hasserjian, J. Thiele, M.J. Borowitz, M.M. Le Beau, C. D. Bloomfield, M. Cazzola, J.W. Vardiman, The 2016 revision to the World Health Organization classification of myeloid neoplasms and acute leukemia, Blood 127 (20) (2016) 2391–2405, https://doi.org/10.1182/blood-2016-03-643544.
[9] N.J. Short, M. Konopleva, T.M. Kadia, G. Borthakur, F. Ravandi, C.D. DiNardo, N. Daver, Advances in the Treatment of Acute Myeloid Leukemia: New Drugs and New Challenges, Cancer Discov. 10 (4) (2020) 506–525, https://doi.org/10.1158/2159-8290.Cd-19-1011.
[10] H. Kiyoi, N. Kawashima, Y. Ishikawa, FLT3 mutations in acute myeloid leukemia: Therapeutic paradigm beyond inhibitor development, Cancer Sci. 111 (2) (2020) 312–322, https://doi.org/10.1111/cas.14274.
[11] B.W. Parcells, A.K. Ikeda, T. Simms-Waldrip, T.B. Moore, K.M. Sakamoto, FMS-like tyrosine kinase 3 in normal hematopoiesis and acute myeloid leukemia, Stem Cells 24 (5) (2006) 1174–1184, https://doi.org/10.1634/stemcells.2005-0519.
[12] R. Swords, C. Freeman, F. Giles, Targeting the FMS-like tyrosine kinase 3 in acute myeloid leukemia, Leukemia 26 (10) (2012) 2176–2185, https://doi.org/10.1038/leu.2012.114.
[13] M. Tecik, A. Adan, Therapeutic targeting of FLT3 in acute myeloid leukemia: current status and novel approaches, Onco Targets Ther. 15 (2022) 1449–1478, https://doi.org/10.2147/ott.S384293.
[14] P.D. Kottaridis, R.E. Gale, D.C. Linch, Flt3 mutations and leukaemia, Br. J. Haematol. 122 (4) (2003) 523–538, https://doi.org/10.1046/j.1365-2141.2003.04500.x.
[15] J. Yu, P.Y.Z. Jiang, H. Sun, X. Zhang, Z. Jiang, Y. Li, Y. Song, Advances in targeted therapy for acute myeloid leukemia, Biomark. Res. 8 (1) (2020) 17, https://doi.org/10.1186/s40364-020-00196-2.

[16] M. Mori, N. Kaneko, Y. Ueno, M. Yamada, R. Tanaka, R. Saito, I. Shimada, K. Mori, S. Kuromitsu, Gilteritinib, a FLT3/AXL inhibitor, shows antileukemic activity in mouse models of FLT3 mutated acute myeloid leukemia, Invest N. Drugs 35 (5) (2017) 556–565, https://doi.org/10.1007/s10637-017-0470-z.
[17] R. Roskoski, The role of small molecule Flt3 receptor protein-tyrosine kinase inhibitors in the treatment of Flt3-positive acute myelogenous leukemias, Pharmacol. Res. 155 (2020), 104725, https://doi.org/10.1016/j.phrs.2020.104725.
[18] A.E. Perl, G. Martinelli, J.E. Cortes, A. Neubauer, E. Berman, S. Paolini, P. Montesinos, M.R. Baer, R.A. Larson, C. Ustun, F. Fabbiano, H.P. Erba, A. Di Stasi, R. Stuart, R. Olin, M. Kasner, F. Ciceri, W.C. Chou, N. Podoltsev, C. Recher, H. Yokoyama, N. Hosono, S.S. Yoon, J.H. Lee, T. Pardee, A.T. Fathi, C. Liu, N. Hasabou, X. Liu, E. Bahceci, M.J. Levis, Gilteritinib or Chemotherapy for Relapsed or Refractory FLT3-Mutated AML, N. Engl. J. Med 381 (18) (2019) 1728–1740, https://doi.org/10.1056/NEJMoa1902688.
[19] M. Levis, Midostaurin approved for FLT3-mutated AML, Blood 129 (26) (2017) 3403–3406, https://doi.org/10.1182/blood-2017-05-782292.
[20] N. Daver, J. Cortes, F. Ravandi, K.P. Patel, J.A. Burger, M. Konopleva, H. Kantarjian, Secondary mutations as mediators of resistance to targeted therapy in leukemia, Blood 125 (21) (2015) 3236–3245, https://doi.org/10.1182/blood-2014-10-605808.
[21] P. Wang, X. Xiao, Y. Zhang, B. Zhang, D. Li, M. Liu, X. Xie, C. Liu, P. Liu, R. Ren, A dual inhibitor overcomes drug-resistant FLT3-ITD acute myeloid leukemia, J. Hematol. Oncol. 14 (1) (2021) 105, https://doi.org/10.1186/s13045-021-01098-y.
[22] P.-Y. Dumas, E. Raffoux, E. Bérard, S. Bertoli, M.-A. Hospital, M. Heiblig, Y. Desbrosses, C. Bonmati, C. Pautas, J. Lambert, C. Orvain, A. Banos, F. Pasquier, P. Peterlin, T. Marchand, M. Uzunov, J. Frayfer, P. Turlure, T. Cluzeau, E. Jourdan, C. Himberlin, E. Tavernier, A. Villate, S. Haiat, M.-L. Chretien, M. Carre, S. Chantepie, I. Vaida, M. Wemeau, S. Chebrek, G. Guillerm, R. Guièze, H. Debarri, E. Gehlkopf, K. Laribi, A. Marcais, A. Santagostino, M.-C. Béné, A. Mineur, A. Pigneux, H. Dombret, C. Récher, Gilteritinib activity in refractory or relapsed FLT3-mutated acute myeloid leukemia patients previously treated by intensive chemotherapy and midostaurin: a study from the French AML Intergroup ALFA/FILO, Leukemia 37 (1) (2023) 91–101, https://doi.org/10.1038/s41375-022-01742-7.
[23] T.M. Weis, B.L. Marini, D.L. Bixby, A.J. Perissinotti, Clinical considerations for the use of FLT3 inhibitors in acute myeloid leukemia, Crit. Rev. Oncol. /Hematol. 141 (2019) 125–138, https://doi.org/10.1016/j.critrevonc.2019.06.011.
[24] E.D. Pulte, K.J. Norsworthy, Y. Wang, Q. Xu, H. Qosa, R. Gudi, D. Przepiorka, W. Fu, O.O. Okusanya, K.B. Goldberg, R.A. De Claro, A.T. Farrell, R. Pazdur, FDA Approval Summary: Gilteritinib for Relapsed or Refractory Acute Myeloid Leukemia with a FLT3 Mutation, Clin. Cancer Res. 27 (13) (2021) 3515–3521, https://doi.org/10.1158/1078-0432.Ccr-20-4271.
[25] M. Takahashi, K. Kawai, N. Asai, Roles of the RET proto-oncogene in cancer and development, Jma J. 3 (3) (2020) 175–181, https://doi.org/10.31662/jmaj.2020-0021.
[26] E. Arighi, M.G. Borrello, H. Sariola, RET tyrosine kinase signaling in development and cancer, Cytokine Growth Factor Rev. 16 (4) (2005) 441–467, https://doi.org/10.1016/j.cytogfr.2005.05.010.
[27] V. Subbiah, V. Velcheti, B.B. Tuch, K. Ebata, N.L. Busaidy, M.E. Cabanillas, L. J. Wirth, S. Stock, S. Smith, V. Lauriault, S. Corsi-Travali, D. Henry, M. Burkard, R. Hamor, K. Bouhana, S. Winski, R.D. Wallace, D. Hartley, S. Rhodes, M. Reddy, B. J. Brandhuber, S. Andrews, S.M. Rothenberg, A. Drilon, Selective RET kinase inhibition for patients with RET-altered cancers, Ann. Oncol. 29 (8) (2018) 1869–1876, https://doi.org/10.1093/annonc/mdy137.
[28] A.T. Regua, M. Najjar, H.-W. Lo, RET signaling pathway and RET inhibitors in human cancer, Front. Oncol. 12 (2022), https://doi.org/10.3389/fonc.2022.932353.
[29] K.Z. Thein, V. Velcheti, B.H.M. Mooers, J. Wu, V. Subbiah, Precision therapy for RET-altered cancers with RET inhibitors, Trends Cancer 7 (12) (2021) 1074–1088, https://doi.org/10.1016/j.trecan.2021.07.003.
[30] M. Yu, J. Wang, D. Ma, S. Chen, X. Lin, Q. Fang, N. Zhe, HO-1, RET and PML as possible markers for risk stratification of acute myelocytic leukemia and prognostic evaluation, Oncol. Lett. 10 (5) (2015) 3137–3144, https://doi.org/10.3892/ol.2015.3644.
[31] S. Rudat, A. Pfaus, Y.Y. Cheng, J. Holtmann, J.M. Ellegast, C. Bühler, D. D. Marcantonio, E. Martinez, S. Göllner, C. Wickenhauser, C. Müller-Tidow, C. Lutz, L. Bullinger, M.D. Milsom, S.M. Sykes, S. Fröhling, C. Scholl, RET-mediated autophagy suppression as targetable co-dependence in acute myeloid leukemia, Leukemia 32 (10) (2018) 2189–2202, https://doi.org/10.1038/s41375-018-0102-4.
[32] W. Seo, P. Silwal, I.-C. Song, E.-K. Jo, The dual role of autophagy in acute myeloid leukemia, J. Hematol. Oncol. 15 (1) (2022) 51, https://doi.org/10.1186/s13045-022-01262-y.
[33] W. Du, A. Xu, Y. Huang, J. Cao, H. Zhu, B. Yang, X. Shao, Q. He, M. Ying, The role of autophagy in targeted therapy for acute myeloid leukemia, Autophagy 17 (10) (2021) 2665–2679, https://doi.org/10.1080/15548627.2020.1822628.
[34] C. Larrue, E. Saland, H. Boutzen, F. Vergez, M. David, C. Joffre, M.A. Hospital, J. Tamburini, E. Delabesse, S. Manenti, J.E. Sarry, C. Récher, Proteasome inhibitors induce FLT3-ITD degradation through autophagy in AML cells, Blood 127 (7) (2016) 882–892, https://doi.org/10.1182/blood-2015-05-646497.
[35] S.P. Zhang, Y.N. Niu, N. Yuan, A.H. Zhang, D. Chao, Q.P. Xu, L.J. Wang, X. G. Zhang, W.L. Zhao, Y. Zhao, J.R. Wang, Role of autophagy in acute myeloid leukemia therapy, Chin. J. Cancer 32 (3) (2013) 130–135, https://doi.org/10.5732/cjc.012.10073.
[36] P.R. Halliday, C.M. Blakely, T.G. Bivona, Emerging Targeted Therapies for the Treatment of Non-small Cell Lung Cancer, Curr. Oncol. Rep. 21 (3) (2019) 21, https://doi.org/10.1007/s11912-019-0770-x.
[37] K.M. Ndolo, S.J. An, K.R. Park, H.J. Lee, K.B. Yoon, Y.C. Kim, S.Y. Han, Discovery of an Indirubin Derivative as a Novel c-Met Kinase Inhibitor with In Vitro Anti-Tumor Effects, Biomol. Ther. (Seoul.) 27 (2) (2019) 216–221, https://doi.org/10.4062/biomolther.2018.091.
[38] H.J. Lee, P. Jeong, Y. Moon, J. Choi, J.D. Heo, Y.C. Kim, S.Y. Han, Characterization of LDD-2633 as a Novel RET Kinase Inhibitor with Anti-Tumor Effects in Thyroid Cancer, Pharm. (Basel) 14 (1) (2021), https://doi.org/10.3390/ph14010038.
[39] M.E. Moreno-Fernandez, M. Damen, S. Divanovic, A protocol for isolation of primary human immune cells from the liver and mesenteric white adipose tissue biopsies, STAR Protoc. 2 (4) (2021), 100937, https://doi.org/10.1016/j.xpro.2021.100937.
[40] P. Jeong, Y. Moon, J.-H. Lee, S.-D. Lee, J. Park, J. Lee, J. Kim, H.J. Lee, N.Y. Kim, J. Choi, J.D. Heo, J.E. Shin, H.W. Park, Y.-G. Kim, S.-Y. Han, Y.-C. Kim, Discovery of orally active indirubin-3′-oxime derivatives as potent type 1 FLT3 inhibitors for acute myeloid leukemia, Eur. J. Med. Chem. 195 (2020), 112205, https://doi.org/10.1016/j.ejmech.2020.112205.
[41] T. Grafone, M. Palmisano, C. Nicci, S. Storti, An overview on the role of FLT3-tyrosine kinase receptor in acute myeloid leukemia: biology and treatment, Oncol. Rev. 6 (1) (2012), e8, https://doi.org/10.4081/oncol.2012.e8.
[42] R. Zhu, L. Li, B. Nguyen, J. Seo, M. Wu, T. Seale, M. Levis, A. Duffield, Y. Hu, D. Small, FLT3 tyrosine kinase inhibitors synergize with BCL-2 inhibition to eliminate FLT3/ITD acute leukemia cells through BIM activation, Signal Transduct. Target Ther. 6 (1) (2021) 186, https://doi.org/10.1038/s41392-021-00578-4.
[43] Y. Qiu, Y. Li, M. Chai, H. Hua, R. Wang, S. Waxman, Y. Jing, The GSK3β/Mcl-1 axis is regulated by both FLT3-ITD and Axl and determines the apoptosis induction abilities of FLT3-ITD inhibitors, Cell Death Discov. 9 (1) (2023) 44, https://doi.org/10.1038/s41420-023-01317-0.
[44] A.J. James, C.C. Smith, M. Litzow, A.E. Perl, J.K. Altman, D. Shepard, T. Kadokura, K. Souda, M. Patton, Z. Lu, C. Liu, S. Moy, M.J. Levis, E. Bahceci, Pharmacokinetic Profile of Gilteritinib: A Novel FLT-3 Tyrosine Kinase Inhibitor, Clin. Pharmacokinet. 59 (10) (2020) 1273–1290, https://doi.org/10.1007/s40262-020-00888-w.
[45] M. Loi, D. Di Paolo, P. Becherini, A. Zorzoli, P. Perri, R. Carosio, M. Cilli, D. Ribatti, C. Brignole, G. Pagnan, M. Ponzoni, F. Pastorino, The use of the orthotopic model to validate antivascular therapies for cancer, Int J. Dev. Biol. 55(4-5) ((2011) 547–555, https://doi.org/10.1387/ijdb.103230ml.
[46] D. Ribatti, G. Mangialardi, A. Vacca, Stephen Paget and the 'seed and soil' theory of metastatic dissemination, Clin. Exp. Med 6 (4) (2006) 145–149, https://doi.org/10.1007/s10238-006-0117-4.
[47] X. Gui, M. Deng, H. Song, Y. Chen, J. Xie, Z. Li, L. He, F. Huang, Y. Xu, Y. Anami, H. Yu, C. Yu, L. Li, Z. Yuan, X. Xu, Q. Wang, Y. Chai, T. Huang, Y. Shi, K. Tsuchikama, X.C. Liao, N. Xia, G.F. Gao, N. Zhang, C.C. Zhang, Z. An, Disrupting LILRB4/APOE Interaction by an Efficacious Humanized Antibody Reverses T-cell Suppression and Blocks AML Development, Cancer Immunol. Res 7 (8) (2019) 1244–1257, https://doi.org/10.1158/2326-6066.Cir-19-0036.
[48] V. Pallarès, U. Unzueta, A. Falgàs, L. Sánchez-García, N. Serna, A. Gallardo, G. A. Morris, L. Alba-Castellón, P. Álamo, J. Sierra, A. Villaverde, E. Vázquez, I. Casanova, R. Mangues, An Auristatin nanoconjugate targeting CXCR4+ leukemic cells blocks acute myeloid leukemia dissemination, J. Hematol. Oncol. 13 (1) (2020) 36, https://doi.org/10.1186/s13045-020-00863-9.
[49] S.S. Ge, S.B. Liu, S.L. Xue, Developments and challenges of FLT3 inhibitors in acute myeloid leukemia, Front Oncol. 12 (2022), 996438, https://doi.org/10.3389/fonc.2022.996438.
[50] C. Kang, H.A. Blair, Gilteritinib: A Review in Relapsed or Refractory FLT3-Mutated Acute Myeloid Leukaemia, Target. Oncol. 15 (5) (2020) 681–689, https://doi.org/10.1007/s11523-020-00749-3.
[51] Y. Xiang, Z. Guo, P. Zhu, J. Chen, Y. Huang, Traditional Chinese medicine as a cancer treatment: Modern perspectives of ancient but advanced science, Cancer Med 8 (5) (2019) 1958–1975, https://doi.org/10.1002/cam4.2108.
[52] K. Wang, Q. Chen, Y. Shao, S. Yin, C. Liu, Y. Liu, R. Wang, T. Wang, Y. Qiu, H. Yu, Anticancer activities of TCM and their active components against tumor metastasis, Biomed. Pharmacother. 133 (2021), 111044, https://doi.org/10.1016/j.biopha.2020.111044.
[53] L. Yang, X. Li, W. Huang, X. Rao, Y. Lai, Pharmacological properties of indirubin and its derivatives, Biomed. Pharmacother. 151 (2022), 113112, https://doi.org/10.1016/j.biopha.2022.113112.
[54] T. Blažević, E.H. Heiss, A.G. Atanasov, J.M. Breuss, V.M. Dirsch, P. Uhrin, Indirubin and Indirubin Derivatives for Counteracting Proliferative Diseases, Evid. Based Complement Altern. Med 2015 (2015), 654098, https://doi.org/10.1155/2015/654098.
[55] Y. Qi-Yue, Z. Ting, H. Ya-Nan, H. Sheng-Jie, D. Xuan, H. Li, X. Chun-Guang, From natural dye to herbal medicine: A systematic review of chemical constituents, pharmacological effects and clinical applications of indigo naturalis, Chin. Med. 15 (1) (2020) 1–13, https://doi.org/10.1186/s13020-020-00406-x.
[56] J. Rygaard, C.O. Poulsen, Heterotransplantation of a human malignant tumour to "Nude" mice, Acta Pathol. Microbiol. Scand. 77 (4) (1969) 758–760, https://doi.org/10.1111/j.1699-0463.1969.tb04520.x.
[57] C.R. Ireson, M.S. Alavijeh, A.M. Palmer, E.R. Fowler, H.J. Jones, The role of mouse tumour models in the discovery and development of anticancer drugs, Br. J. Cancer 121 (2) (2019) 101–108, https://doi.org/10.1038/s41416-019-0495-5.
[58] D.H. Lum, C. Matsen, A.L. Welm, B.E. Welm, Overview of human primary tumorgraft models: comparisons with traditional oncology preclinical models and the clinical relevance and utility of primary tumorgrafts in basic and translational

oncology research (Unit), Curr. Protoc. Pharm. Chapter 14 14 (2012) 22, https://doi.org/10.1002/0471141755.ph1422s59.
[59] S. Paget, The distribution of secondary growths in cancer of the breast. 1889, Cancer Metastas-.-. Rev. 8 (2) (1989) 98–101, https://doi.org/10.1016/S0140-6736(00)49915-0.
[60] R.M. Hoffman, Patient-derived orthotopic xenografts: better mimic of metastasis than subcutaneous xenografts, Nat. Rev. Cancer 15 (8) (2015) 451–452, https://doi.org/10.1038/nrc3972.
[61] T. Murakami, Absorption sites of orally administered drugs in the small intestine, Expert Opin. Drug Discov. 12 (12) (2017) 1219–1232, https://doi.org/10.1080/17460441.2017.1378176.